Geodynamics of synconvergent extension and tectonic mode switching: Constraints from the Sevier-Laramide orogen

Michael L. Wells,[1] Thomas D. Hoisch,[2] Alicia M. Cruz-Uribe,[3] and Jeffrey D. Vervoort[4]

Received 16 March 2011; revised 10 October 2011; accepted 7 November 2011; published 13 January 2012.

[1] Many orogenic belts experience alternations in shortening and extension (tectonic mode switches) during continuous plate convergence. The geodynamics of such alternations are not well understood. We present a record of Late Cretaceous to Eocene alternations of shortening and extension from the interior of the retroarc Sevier-Laramide orogen of the western United States. We integrate new Lu-Hf garnet geochronometry with revised PT paths utilizing differential thermobarometry combined with isochemical G-minimization plots, and monazite Th-Pb inclusion geochronometry to produce a well-constrained "M" shaped PTt path. Two burial events (86 and 65 Ma) are separated by ~3 kbar of decompression. The first burial episode is Late Cretaceous, records a 2 kbar pressure increase at ~515–550 °C and is dated by a Lu-Hf garnet isochron age of 85.5 ± 1.9 Ma (2σ); the second burial episode records ~1 kbar of pressure increase at ~585–615 °C, and is dated by radially decreasing Th-Pb ages of monazite inclusions in garnet between ~65 and 45 Ma. We propose a synconvergent lithospheric delamination cycle, superimposed on a dynamic orogenic wedge, as a viable mechanism. Wedge tapers may evolve from critical to subcritical (amplification), to supercritical (separation), and back to subcritical (re-equilibration) owing to elevation changes resulting from isostatic adjustments during the amplification and separation of Rayleigh-Taylor instabilities, and post-separation thermal and rheological re-equilibration. For the Sevier-Laramide hinterland, the sequence of Late Cretaceous delamination, low-angle subduction, and slab rollback/foundering during continued plate convergence explains the burial-exhumation-burial-exhumation record and the "M-shaped" PTt path.

Citation: Wells, M. L., T. D. Hoisch, A. M. Cruz-Uribe, and J. D. Vervoort (2012), Geodynamics of synconvergent extension and tectonic mode switching: Constraints from the Sevier-Laramide orogen, *Tectonics*, *31*, TC1002, doi:10.1029/2011TC002913.

1. Introduction

[2] The widespread recognition of extension within orogenic belts at active and ancient convergent plate margins has shown that synconvergent extension is a common and important process during orogenesis [e.g., *Dalmayrac and Molnar*, 1981; *Burchfiel and Royden*, 1985; *Wallis et al.*, 1993]. Extension commonly follows shortening in the terminal phase or late in orogenesis [e.g., *Dewey*, 1988; *Vanderhaeghe and Teyssier*, 2001]. In many cases, however, renewed shortening follows synconvergent extension, and complex deformation and metamorphic histories involving alternations in shortening/burial and extension/exhumation are increasingly recognized [e.g., *Platt*, 1986; *Rawling and Lister*, 1999; *Collins*, 2002]. Such alternations — elsewhere referred to as tectonic switching [*Collins*, 2002], deformation mode switching [*Beltrando et al.*, 2008] or tectonic mode switching [*Lister et al.*, 2001] — challenge the simple model of an orogenic cycle that results in a clockwise PT path [*England and Thompson*, 1984], characterized by shortening and tectonic burial, radiogenic heating, and extensional and erosional exhumation. The geodynamics of kinematic alternations, although a well-recognized phenomenon, are not well understood.

[3] Kinematic alternations in shortening and extension in the Lachlan orogen [*Collins*, 2002], New Caledonia [*Rawling and Lister*, 1999], western Alps [*Beltrando et al.*, 2007], and Aegean [*Lister et al.*, 2001] have been interpreted as resulting from slab rollback (trench retreat) inducing extension in the overriding plate punctuated by episodes of shortening and lithospheric thickening. Shortening results from accretion and/or interactions between the overriding plate and embedded continental fragments and oceanic

[1]Department of Geosciences, University of Nevada, Las Vegas, Las Vegas, Nevada, USA.
[2]Department of Geology, Northern Arizona University, Flagstaff, Arizona, USA.
[3]Department of Geosciences, Pennsylvania State University, University Park, Pennsylvania, USA.
[4]School of Earth and Environmental Sciences, Washington State University, Pullman, Washington, USA.

0278-7407/12/2011TC002913

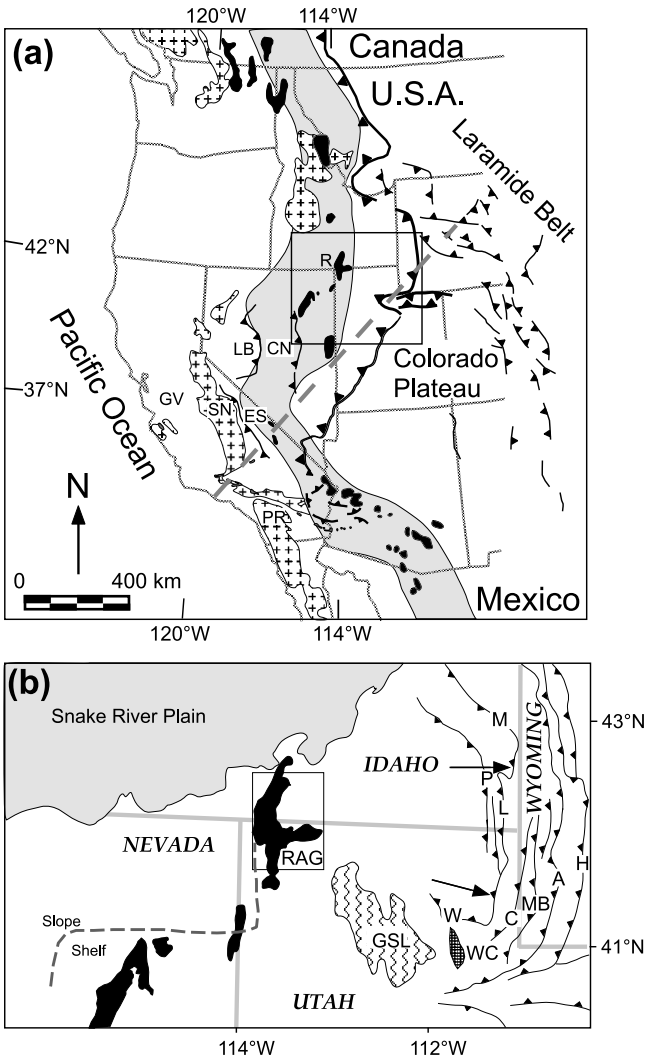

Figure 1. (a) Simplified tectonic map of the western U.S., showing selected Late Mesozoic to early Tertiary tectonic features of the retroarc and location of Figure 1b. Cretaceous magmatic arc shown by cross pattern. Belt of muscovite granites (gray fill) after *Miller and Bradfish* [1980]. Metamorphic core complexes (black fill) approximate axis of maximum crustal thickening. Leading edge of Sevier fold-thrust belt shown, and fold-thrust uplifts of the Laramide Rocky Mountain foreland. Dashed line shows position of inferred segment boundary in Farallon slab between shallower angle (south) and steeper angle (north) subduction, after *Saleeby* [2003]. GV, Great Valley forearc basin; PR, Peninsular Ranges batholith; R, Raft River-Albion-Grouse Creek core complex; SN, Sierra Nevada batholith; LB, Luning-Fencemaker belt; CN, Central Nevada thrust belt; ES, East Sierran thrust system. (b) Simplified tectonic map of the Idaho-Utah-Wyoming sector of the Sevier fold thrust belt and its hinterland. Thrusts in thrust belt include A, Absaroka; C, Crawford; H, Hogsback; L, Laketown; MB, Medicine Butte; M, Meade; P, Paris; W, Willard. WC is Wasatch culmination, a basement-involved antiformal stack. GSL is Great Salt Lake. Arrows represent transport direction. Early Paleozoic shelf-slope break from *Miller et al.* [1991].

plateaus in the subducting oceanic lithosphere. In contrast, an episode of Late Cretaceous synconvergent extension, leading to a kinematic alternation of shortening-extension-shortening in the hinterland of the Sevier-Laramide orogenic belt [*Wells*, 1997; *Hoisch et al.*, 2002], has been interpreted to have occurred in the absence of slab rollback and to be triggered by lithospheric mantle delamination [*Wells and Hoisch*, 2008].

[4] The Sevier and Laramide orogens of the western United States (Figure 1) are Late Mesozoic to early Cenozoic retroarc belts of crustal shortening that are components of the larger Cordilleran orogen [e.g., *Allmendinger*, 1992; *DeCelles*, 2004]. Exposures of upper greenschist- to upper amphibolite-facies metamorphic rocks exhumed beneath low-angle normal faults in metamorphic core complexes (MCC) of the hinterland, such as the Raft River-Albion-Grouse Creek (RAG) MCC, provide windows into deep level tectonic processes of the Sevier-Laramide orogen. In the metamorphic infrastructure of the core complexes, it is common for the early shortening recorded in deformation fabrics and stratigraphic juxtapositions to be obscured by extensional flow fabrics [e.g., *Camilleri*, 1998; *Wells et al.*, 2008]. This leaves the metamorphic record as the strongest evidence for large magnitude tectonic burial due to crustal shortening [*Camilleri and Chamberlain*, 1997; *Lewis et al.*, 1999; *McGrew et al.*, 2000; *Harris et al.*, 2007].

[5] The deformation and metamorphic history preserved in the RAG MCC has been interpreted to record alternating shortening and extension during Sevier orogenesis (Table 1 and Figure 2) [*Wells*, 1997; *Hoisch et al.*, 2002; *Harris et al.*, 2007]. The absolute timing of several of the shortening and extension events, however, has not been previously well determined. Here we present new Lu-Hf garnet geochronometry from middle to upper amphibolite-facies pelitic schist from which we have previously determined PT paths [*Hoisch et al.*, 2002; *Harris et al.*, 2007]. Additionally, we revise the PT paths through an integrated approach of differential thermobarometry (Gibbs method) and G-minimization. These new data are combined with previously published monazite Th-Pb inclusion geochronometry [*Hoisch et al.*, 2008] and field geologic observations [*Wells*, 1997; *Wells et al.*, 1998, 2008] to provide a more complete history of Late Cretaceous to early Tertiary kinematic alternations in the hinterland of the Sevier-Laramide orogen. With the revised chronology, we evaluate the causes of tectonic mode switches in this non-collisional orogen. Building on the delamination model introduced by *Wells and Hoisch* [2008], we propose a more comprehensive geodynamic model of a synconvergent lithospheric delamination cycle, superimposed on a dynamic orogenic wedge, as a viable mechanism. As a part of the delamination cycle, we suggest that subsidence during growth of a Raleigh-Taylor instability in the mantle lithosphere, and its associated convergent flow, can induce renewed and focused shortening in the interior of orogenic wedges. As an alternative to episodic slab rollback, we propose that episodic delamination of the lower crust and/or mantle lithosphere in the arc and retroarc can lead to episodic extension during continued subduction. Such cyclic delamination has recently been proposed for Cordilleran orogenic

Table 1. Sequence of Mesozoic to Early Cenozoic Deformations as Proposed in This and Previous Studies for the Footwall to the Basin-Elba Thrust Fault, Western Raft River, Northern Grouse Creek and Albion Mountains

Tectonic Event	Structure and Kinematics	Interpretation	Timing	Metamorphism
M_1	1st motion on Basin-Elba fault?	Contraction	149–132 Ma, Lu-Hf garnet[a,b]	Metamorphism of schist of Mahogany Peaks; Isothermal P increase[a,b,c]
D_1	Top-to-north shearing[d,e]	Orogen-parallel extension[d]	105 ± 6 Ma[d]	
M_2	Reactivation of Basin-Elba fault	Contraction	86 Ma, Lu-Hf garnet[f]	Metamorphism of schist of Stevens Springs; Isothermal P increase (segment 1)[c,g]
D_2	Emigrant Spring and Mahogany Peaks Fault	Extension[h,i]	<90, >60 Ma[i] <86, >65 Ma[f,j]	Inferred decompression P-T path[f,g]
D_3 and M_3	Recumbent folding and reactivation of Basin-Elba fault	Contraction[f,h]	65–45 Ma[j]	P increase (segment 3)[c,g]
D_{4A}	Top-to-WNW shearing Middle Mountain shear zone	Extension[k]	Late Eocene[k] 45–37 Ma	

[a] *Cruz-Uribe* [2008].
[b] *Cruz-Uribe et al.* [2008].
[c] *Harris et al.* [2007].
[d] *Wells et al.* [2008].
[e] *Malavieille* [1987].
[f] This study.
[g] *Hoisch et al.* [2002].
[h] *Wells* [1997].
[i] *Wells et al.* [1998].
[j] *Hoisch et al.* [2008].
[k] *Wells et al.* [2000].

systems, following episodic high flux magmatic events in arcs [*DeCelles et al.*, 2009].

2. Geologic Setting of Sevier-Laramide Orogen

[6] Retroarc shortening during the Sevier and Laramide orogenies is generally attributed to Andean-style convergent tectonism during subduction of the Farallon plate beneath western North America [*Jordan et al.*, 1983; *DeCelles*, 2004]. Subduction was continuous from the latest Jurassic until the late Oligocene to Miocene time-transgressive initiation of the San Andreas transform system [e.g., *Atwater and Stock*, 1998]. The orthogonal component of plate convergence increased during the Late Cretaceous — at the onset of the Laramide orogeny — broadly coincident with an increase in westward drift of the North American continent during rapid seafloor spreading in the North Atlantic [*Engebretson et al.*, 1985; *Müller et al.*, 1997]. Increasing plate convergence rates, decreasing age of subducted lithosphere, and subduction of an oceanic plateau are thought to have led to a shallowing of the Farallon slab, increased plate coupling, and enhanced shortening [*Henderson et al.*, 1984; *Severinghaus and Atwater*, 1990; *Barth and Schneiderman*, 1996; *Liu et al.*, 2010]. Many geologic observations in western North America are also consistent with Late Cretaceous shallowing of the subterranean Farallon slab in a NE-trending swath from southeastern California to Wyoming, and with the slab remaining shallow until the Early Eocene [*Coney and Reynolds*, 1977; *Bird*, 1984; *Grove et al.*, 2003; *Usui et al.*, 2003; *Liu and Nummedal*, 2004]. A marked decrease in plate convergence rate beginning in the Paleocene led to eventual cessation of Sevier and Laramide shortening [*Engebretson et al.*, 1985; *Constenius*, 1996].

[7] The Sevier-Laramide orogen comprises, from east to west, the Laramide foreland province, the Sevier fold and thrust belt, and the hinterland region. The Sevier fold and thrust belt, north of Las Vegas, Nevada, deforms passive margin sediments of the westward-thickening Cordilleran miogeocline and exhibits a classic thin-skinned structural style [e.g., *Armstrong*, 1968; *Allmendinger*, 1992; *DeCelles and Coogan*, 2006], whereas the Laramide foreland province exhibits discontinuous fold-thrusts that deform Precambrian basement and its thin cratonal Phanerozoic cover [*Allmendinger*, 1992; *Erslev*, 1993] (Figure 1). Between the fold-thrust belt and the Mesozoic magmatic arc lies the hinterland region [*Allmendinger*, 1992], wherein much of the record of Mesozoic shortening is obscured by Eocene to recent crustal extension and associated magmatism of the Basin and Range province [e.g., *Wernicke*, 1992; *Dickinson*, 2002]. Despite the structural and magmatic overprint, studies in the hinterland reveal belts of Mesozoic upper crustal shortening [*Speed et al.*, 1988; *Camilleri and Chamberlain*, 1997; *Taylor et al.*, 2000]. Additionally, a record of crustal shortening is preserved in isolated exposures of locally exhumed greenschist- and amphibolite-facies rocks of Cordilleran MCCs [*Miller et al.*, 1988; *McGrew et al.*, 2000; *Harris et al.*, 2007].

[8] Deformation within the Sevier orogen appears to have progressed in a forward propagating west to east sequence from Jurassic to early Eocene time [*DeCelles*, 2004] (Figure 2), although the age of inception of shortening remains controversial [e.g., *Heller et al.*, 1986; *DeCelles and Currie*, 1996]. Out-of-sequence thrusting and folding is well documented in the foreland fold and thrust belt [*DeCelles and Mitra*, 1995; *DeCelles*, 2004] but more cryptic in the hinterland [*Camilleri and Chamberlain*, 1997; this study] and resulted in shortening internal to the orogenic wedge (Figure 2). Balanced cross sections of the fold and thrust belt indicate the basal décollement to the Sevier orogen restores westward to at least the Utah-Nevada border (pre Basin-and-Range extension) beneath Late Precambrian clastic sedimentary rocks of the Willard and equivalent thrust sheets [e.g., *Royse et al.*, 1975; *Allmendinger*, 1992; *DeCelles and Coogan*, 2006], and is inferred to ramp downward toward the west into Precambrian basement and root in either the lower crust or the asthenosphere beneath the Sierran

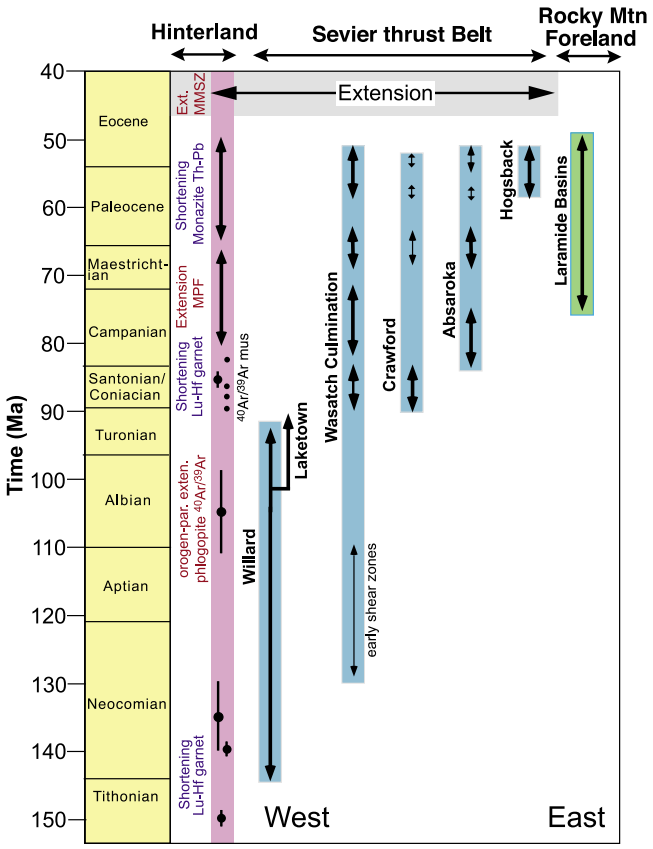

Figure 2. Comparison of timing of events from the hinterland, Sevier fold-thrust belt, and Rocky Mountain foreland, between 41°N and 43°N latitude. Hinterland structural sequence from RAG MCC, with details and references in Table 1. Thrust motion chronology in fold-thrust belt from *DeCelles* [1994, 2004] and *Yonkee* [1992]. Timing of deformation in Rocky Mountain foreland from *Dickinson et al.* [1988]. Generalized timing of inception of Eocene extension from *Constenius* [1996] and *Wells et al.* [2000]. Lu-Hf garnet ages from *Cruz-Uribe et al.* [2008]; phlogopite $^{40}Ar/^{39}Ar$ ages from strain fringes from *Wells et al.* [2008]. Note age progression of initial deformation from west to east, episodic motion on thrusts in the fold-thrust belt, and Late Cretaceous extension in hinterland coeval with shortening in Wasatch culmination, Absaroka thrust, and early Laramide uplifts and basin formation. MPF, Mahogany Peaks fault.

magmatic arc [*Ducea*, 2001; *DeCelles and Coogan*, 2006; *Wells and Hoisch*, 2008]. During the Late Cretaceous to Eocene, the Sevier orogenic wedge may have been kinematically and dynamically linked with the Laramide foreland province through development of a mid- to lower-crustal décollement in the Laramide foreland, forming an integrated orogenic wedge [*Livaccari*, 1991; *Erslev*, 1993; *DeCelles*, 2004]. Existing data suggest that initial shortening may have propagated from west to east across the Laramide foreland province, although the timing of development of individual paired fold-thrust uplifts and basins remains imprecise [*DeCelles*, 2004, and references therein].

[9] The RAG core complex straddles the area of northwest Utah and southern Idaho and preserves an exceptionally rich tectonic history by virtue of its large areal extent, and exposure of upper amphibolite- to lower greenschist-facies rocks in a tectonically collapsed crustal section. A greatly attenuated Archean through Triassic crustal section is exposed in numerous stacked extensional allochthons whose bounding low-angle faults exhibit younger-over-older stratigraphic juxtapositions (Figure 3). An exception to these relationships occurs in the northern Albion Mountains, where the Basin-Elba fault (Figure 3) — the only preserved thrust fault in the core complex — places a >3.5-km-thick inverted succession of Late Cambrian and Neoproterozoic quartzite and schist of the "quartzite assemblage" over the upright Archean to Ordovician strata of the Raft River Mountains sequence [*Miller*, 1980, 1983]. We have previously interpreted the deformation history preserved in the Raft River Mountains sequence to record alternations in shortening and extension (Table 1) [*Wells*, 1997; *Wells et al.*, 1998, 2008; *Hoisch et al.*, 2002; *Harris et al.*, 2007]. Here we focus on the interval of time from Late Cretaceous to Eocene in which a structural sequence of shortening-extension-shortening-extension is documented (Table 1).

3. Late Cretaceous to Eocene Kinematic Alternations

3.1. Petrologic Evidence for an "M-Shaped" PT Path

[10] Two earlier studies of the schist of Stevens Spring from the Basin Creek area of the northern Grouse Creek Mountains [*Hoisch et al.*, 2002; *Harris et al.*, 2007] determined a prograde pressure-temperature (PT) path consisting of the sequence burial–exhumation–burial. Here we recalculate the PT paths (Figure 4) using a new approach that integrates Gibbs method calculations (program GIBBS described by *Spear et al.* [1991], version of April 30, 2009) with the G-minimization approach of *de Capitani and Petrakakis* [2010] (programs THERIAK and DOMINO, version 01.08.09). Both GIBBS and THERIAK/DOMINO use recent versions of the thermodynamic data set of *Holland and Powell* [1998] (data set *SPaC(2007-Aug)_Thermo.dat* in GIBBS and data set *tcdb55c2* in THERIAK/DOMINO). The Gibbs method requires that initial conditions be specified (pressure, temperature, the phases present, and their modes and compositions). The initial garnet composition values were determined by direct analysis of the garnet core composition, whereas all other initial values including pressure and temperature were inferred from the bulk composition using THERIAK and DOMINO. DOMINO plots equilibrium mineral assemblages, reactions, modes and compositions for specified intervals of pressure and temperature. The location of the garnet core composition on a DOMINO plot is unique and defines the initial pressure and temperature and the initial mineral assemblage. All other initial values were calculated by THERIAK using the initial pressure and temperature. Changes in pressure and temperature (the PT path) were determined using GIBBS by specifying changes in two variables (the monitor parameters) that occurred during garnet growth. The monitor parameters and their values are given by *Hoisch et al.* [2002] and *Harris et al.* [2007]. Bulk compositions were calculated from mineral composition data by *Hoisch et al.* [2002] and *Harris et al.* [2007] along with mineral modes determined from point counts. The paths shown in Figure 4a were shifted slightly (<20°C and

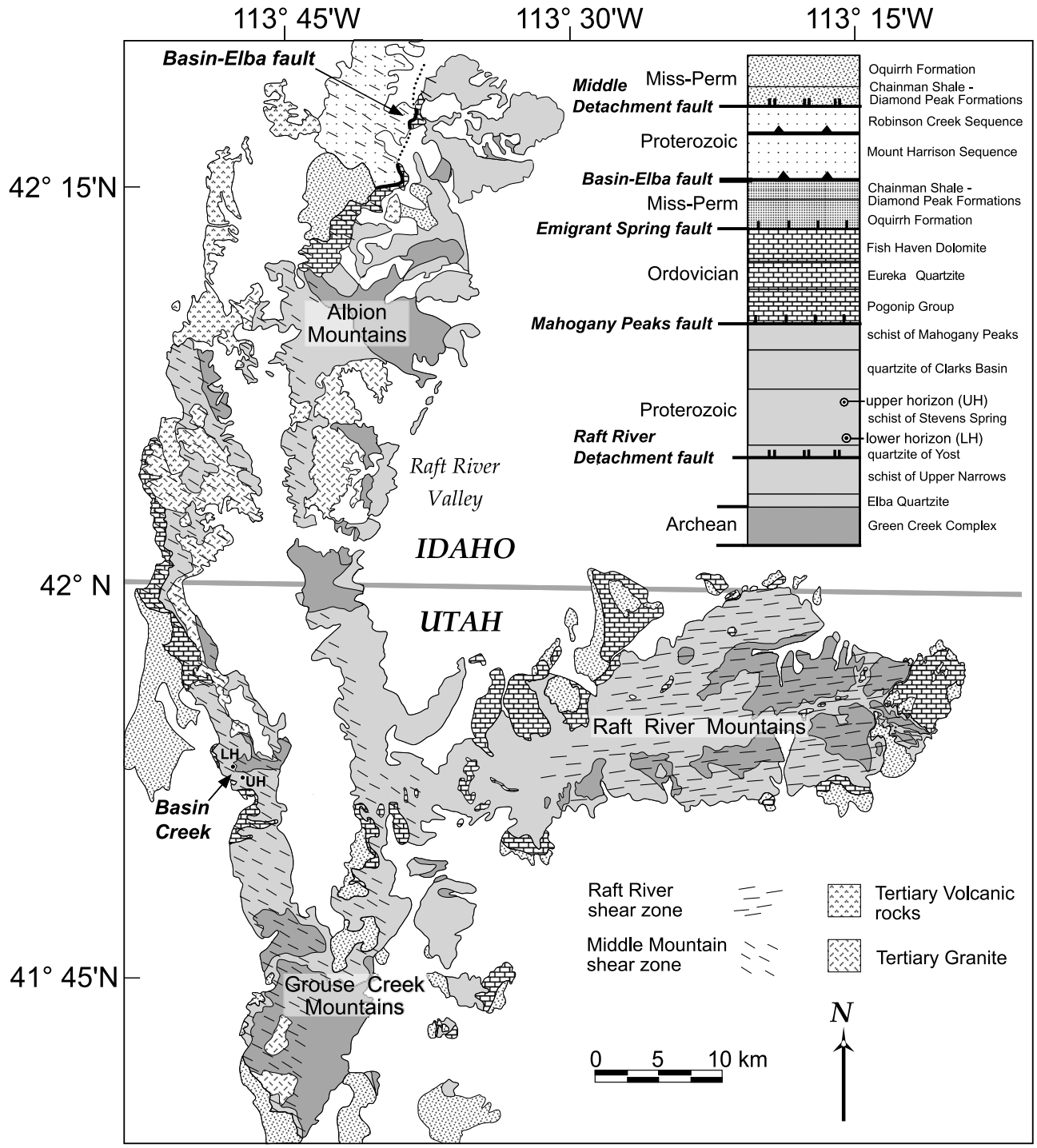

Figure 3. Generalized geologic map of the RAG MCC, modified after *Wells* [1997]. Locations of garnet schist samples in Basin Creek shown; UH are upper horizon samples and LH are lower horizon garnet schist samples of *Hoisch et al.* [2002, 2008] and *Harris et al.* [2007] from the schist of Stevens Spring. The schist lies in the footwall of the Basin-Elba fault, a major thrust fault, which is exposed in the northern Albion Mountains. Note that the schist samples also lie in the footwall of the Mahogany Peaks and Emigrant Spring faults, two low-angle normal faults of probable Late Cretaceous age.

<300 bars) to align similar segments, as described by *Hoisch et al.* [2002] and *Harris et al.* [2007].

[11] Each of the two burial events of the "M-shaped" PT path is recorded by garnet that grew via different reactions due to different bulk compositions. The older garnet growth occurred in the upper horizon of the schist of Stevens Spring at upper greenschist- to lower amphibolite-facies conditions from the breakdown of chlorite (Figures 4a and 5a), and the younger garnet growth occurred in the lower horizon at upper amphibolite facies conditions from the breakdown of

staurolite (Figures 4b and 5b). Exhumation between the two segments of burial was inferred by *Hoisch et al.* [2002] based on the following arguments: (1) early garnet growth took place in the kyanite stability field whereas later garnet growth occurred in the sillimanite stability field; (2) older garnets display prograde modification along cracks and rims whereas younger garnets display retrograde modification along cracks and rims; and (3) the two PT paths cannot be joined without involving a significant drop in pressure.

[12] Direct evidence of the pressure drop following growth of the early formed garnets is present in newly recognized reaction rims on corroded upper horizon garnets (Figure 5a). The reaction rims lack muscovite and consist entirely of plagioclase, biotite and quartz, suggesting a reaction that consumes muscovite and garnet while producing plagioclase and biotite. A path that first increases in temperature then isothermally decreases in pressure yields the observed reaction rim first by growing the garnet larger, then reacting it while consuming muscovite and producing plagioclase and biotite (Figures 4a and 4c).

[13] The late-formed (lower horizon) garnet grew along the PT path shown in Figures 4b and 4c. The garnets are corroded, documenting that they grew beyond what is preserved in the rock, and then underwent partial consumption. A history of garnet growth followed by partial garnet consumption is predicted by the PT path shown in Figures 4b and 4c, in which garnet first grows during staurolite consumption in the absence of sillimanite during an increase of pressure and temperature, then crosses through a narrow field in which sillimanite and garnet are produced and staurolite is consumed, then doubles back through the same field upon cooling, resulting in the production of retrograde staurolite and partial consumption of garnet. Extensional deformation associated with the Middle Mountain shear zone [*Saltzer and Hodges*, 1988; *Wells et al.*, 2000, 2004; *Wells*, 2011] produced strain shadows around garnets as they rotated and underwent corrosion. Varying degrees of rotation resulted in high angles between the external fabric and fabric preserved as inclusion trails in the corroded garnets (Figure 5b) [see also *Strickland et al.*, 2011a]. Retrograde

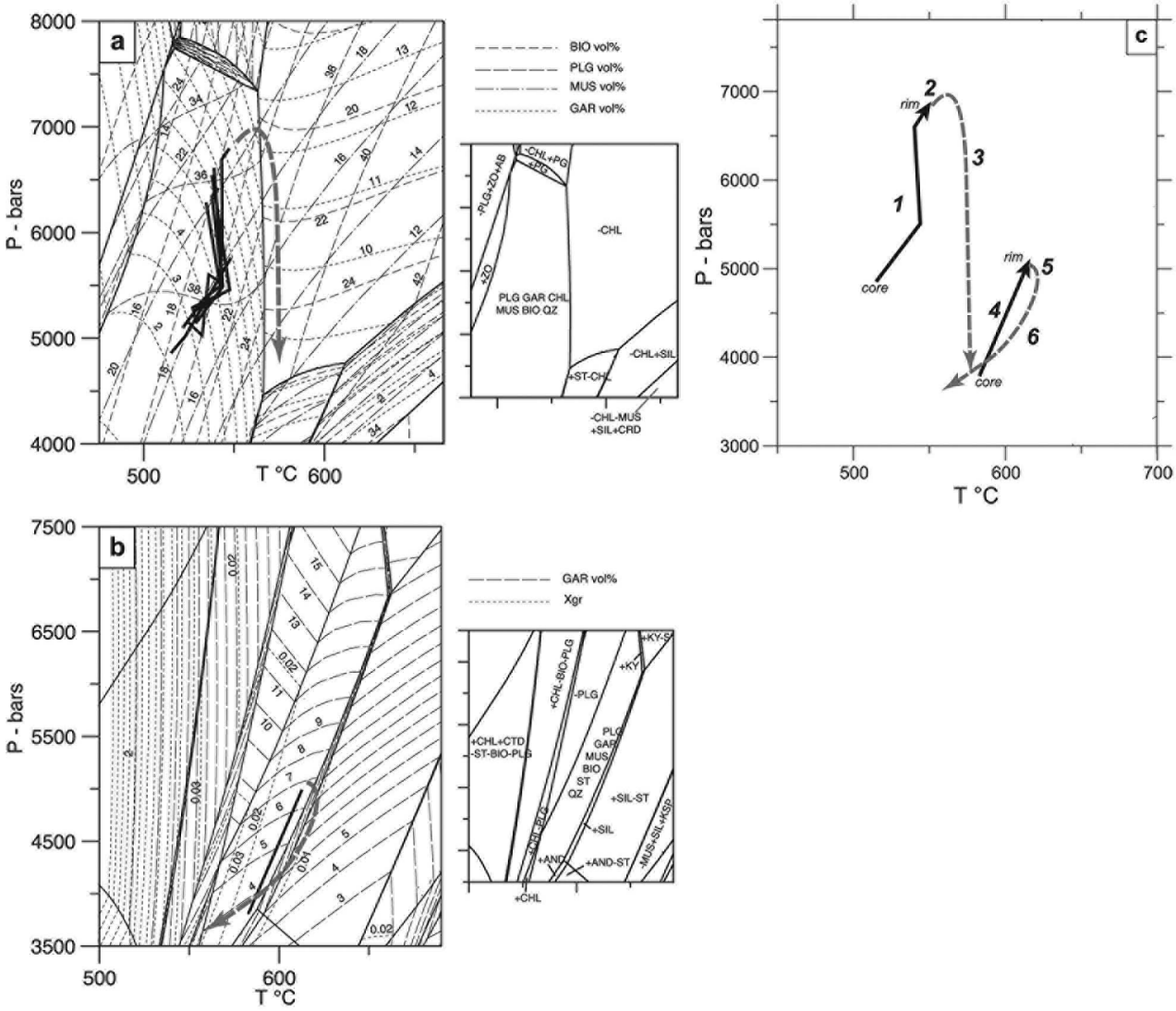

Figure 4

staurolite grains in the matrix contain straight to weakly sigmoidal inclusion trails that vary in concordancy with the external fabric from highly discordant to completely concordant, suggesting they grew synkinematically within the shear fabric (Figure 5b). Retrograde staurolite also nucleated along the margins of corroding garnets (Figure 5b) and within garnet cracks (Figure 5c) [cf. *Strickland et al.*, 2011a]. Our interpretation is that the onset of extensional deformation along the Middle Mountain shear zone occurred late in the growth of the lower horizon garnets.

[14] PT paths generated by this method must be viewed in the context of uncertainties. Although no study has yet approached error propagation in isochemical calculations, some things can be inferred about the likely magnitude of the uncertainties. Studies that have evaluated error propagation in geobarometry calculations yielded uncertainties of ±1–3 kbar [e.g., *Kohn and Spear*, 1991; *Todd*, 1998]. Studies that have evaluated error propagation for the garnet-biotite Fe-Mg exchange equilibrium have yielded estimates of ±25° [*Holdaway*, 2000] and ±50°C [*Kohn and Spear*, 1991]. Errors in geobarometry calculations become inflated at low concentrations of Ca in garnet and plagioclase due to uncertainties in the activity models of grossular in garnet and anorthite in plagioclase. Although G-minimization is a different calculation than thermobarometry, and calculates equilibria that do not involve biotite, garnet or plagioclase, there is no reason to believe it is more precise as it incorporates the same sources of error. In fact it may be less precise because the G-minimization method utilizes additional constraints provided by the bulk composition that contribute additional uncertainties. We assume the uncertainty in the absolute PT placement of reactions and isopleths in isochemical calculations to be no more accurate than thermobarometry calculations, and similarly sensitive to the Ca content of garnet and plagioclase. Although the placement of reactions and isopleths in PT space likely carry large uncertainties, especially with regard to pressure, the relative placement of mineral assemblage fields in PT space appear to be robust.

[15] *Kohn* [1993] evaluated error propagation in differential thermobarometry (i.e., the Gibbs method). He found that the magnitude of changes in pressure and temperature and the value of dP/dT calculated for a path segment from changes in monitor parameters are relatively insensitive to the uncertainties that strongly affect thermobarometry calculations. Thus, for the approach employed in the current study, which combines the two methods, we regard the shape and magnitude of the PT path to be robust, whereas the absolute placement of the PT path in PT space likely carries large uncertainties, especially with regard to pressure.

[16] The composite PT-path (Figure 4c) in the current study is generally similar to the path presented by *Hoisch et al.* [2002] and *Harris et al.* [2007] but differs in some respects. (1) The PT-paths calculated for the upper horizon garnets show greater consistency and improved definition of the composite path. (2) The pressure and temperature conditions corresponding to the initiation of garnet growth in the upper horizon rocks were determined using DOMINO plots to be 515–530°C at 4.8–5.2 kbar whereas *Hoisch et al.* [2002] and *Harris et al.* [2007] assumed 5 kbar and estimated lower initial temperatures (<475°C) by garnet-biotite geothermometry. (3) The initial modes and compositions used in the Gibbs calculation were determined using THERIAK whereas *Hoisch et al.* [2002] and *Harris et al.* [2007] determined initial modes and compositions using an imperfect iterative process. (4) The major decompression is supported by the crossing of garnet mode isopleths in the direction of decreasing mode on a DOMINO plot (Figure 4a) whereas *Hoisch et al.* [2002] and *Harris et al.* [2007] presented no direct evidence for the decompression. The method used to determine the current composite PT-path is therefore more straightforward and self-consistent than for previous versions, and also incorporates additional constraints. Consequently, we consider it to be a better approach and to yield a more robust result.

[17] In summary, petrologic modeling of two bulk compositions of pelitic schist at Basin Creek yields an "M-shaped" PT path (Figure 4c). The first two segments of

Figure 4. PT paths from garnet zoning, from the Basin Creek area of the northern Grouse Creek Mountains, based on data from *Hoisch et al.* [2002] and *Harris et al.* [2007], recalculated using the method described in section 3.1 and plotted on isochemical diagrams [*de Capitani and Petrakakis*, 2010]. Mineral assemblage fields are shown on smaller diagrams; the fields of garnet growth is labeled with the full assemblage and the other fields are labeled with the change in assemblage, "+" indicating a mineral that is added and "−" indicating a mineral that is subtracted. (a) Paths from seven garnets from the upper horizon of the schist of Stevens Spring. Garnet grew primarily from the breakdown of chlorite within the assemblage GAR+CHL+BIO+MUS+PLG+QTZ. Inferred path segment shown by dashed grey line crosses modal isopleths first in the direction of increasing garnet (temperature increase), then in the direction of decreasing garnet and muscovite and increasing plagioclase and biotite (pressure decrease). (b) Path of garnet LH1A from the lower horizon of the schist of Stevens Spring plotted on a pseudosection. Garnet grew primarily from the breakdown of staurolite within the assemblage GAR+ST+BIO+MUS+PLG+QTZ. Inferred path segment shown by dashed grey line crosses staurolite-out sillimanite-in reaction in prograde direction causing further garnet growth, then doubles back over the reaction in the retrograde direction partially consuming garnet and producing staurolite. (c) Complete PT path annotated with the interpretations described in Figures 4a and 4b. 1. PT path for upper horizon garnet growth documenting thrust burial at 85.5 ± 1.9 Ma; 2. Progradation yields further garnet growth; 3. Garnet is partially consumed during decompression to form muscovite-free reaction rims during Late Cretaceous extension; 4. PT path for lower horizon garnet growth during Laramide thrusting dated by co-crystallized monazite inclusions, ∼65 Ma for cores and ∼40 Ma for rims; 5. Further garnet growth as path crosses staurolite-out reaction; 6. Garnet is partially consumed as staurolite-out reaction is crossed in retrograde direction during Eocene extension. Note that the temperature and pressure effects of Oligocene heating during widespread crustal melting and magmatism, and subsequent Late Oligocene to Miocene extension, are not shown for simplicity. Abbreviations: AND (andalusite), BT (biotite), CHL (chlorite), CRD (cordierite), CTD (chloritoid), GAR (garnet), KSP (K-feldspar), KY (kyanite), MUS (muscovite), PG (paragonite), PLG (plagioclase), SIL (sillimanite), Xgr (mole fraction grossular), vol% (volume percent), ZO (zoisite).

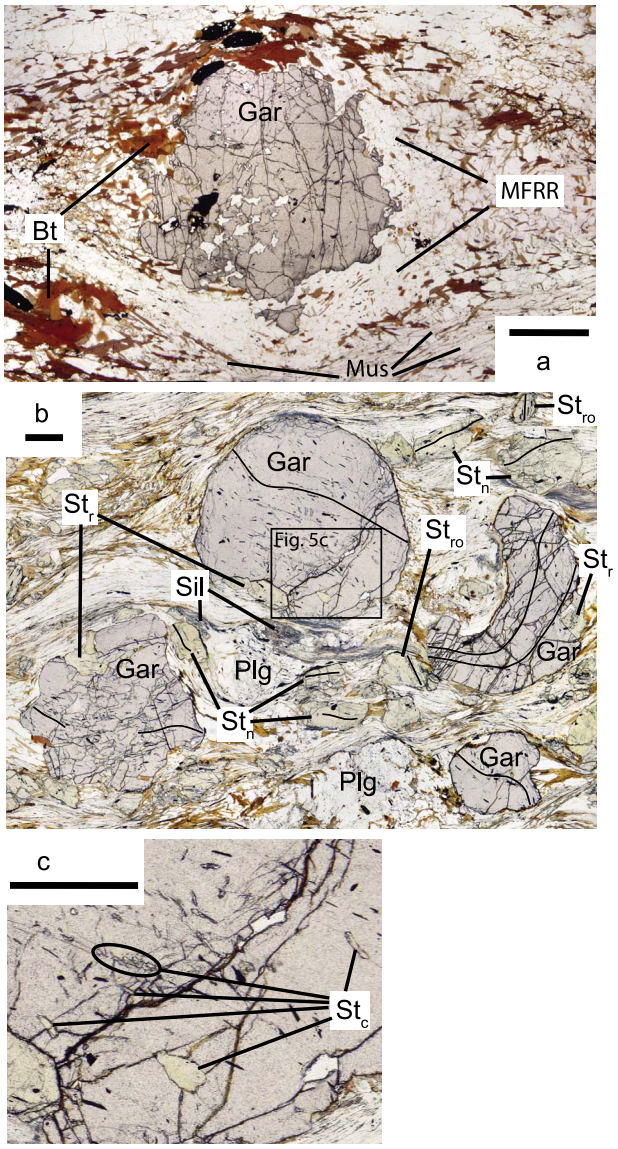

Figure 5. Photomicrographs of samples from which PT paths were determined. Scale bars 1 mm. (a) Sample UH6a, upper horizon of the schist of Stevens Spring (contains older lower temperature garnet). Muscovite-free reaction rims (MFRR) consisting of quartz, plagioclase and biotite surround corroded garnet. (b) Sample LH1, lower horizon of the schist of Stevens Spring (contains younger higher temperature garnet). Relict fabrics preserved as inclusion trails of graphite within selected staurolite and garnet grains are marked with thin solid lines. Shear fabric of the Middle Mountain shear zone wraps around corroded garnets that have been rotated to varying degrees with respect to the external shear fabric. Retrograde staurolite grains nucleated along margins of corroded garnets (St_r) and within matrix consisting of quartz, muscovite and biotite. Both minimally rotated (St_n) and strongly rotated staurolite grains (St_{ro}) overgrow the shear fabric. (c) A portion of a garnet from sample LH1 displaying retrograde staurolite grains nucleated along cracks (St_c). Abbreviations: Bt (biotite), Gar (garnet), Mus (muscovite), Plg (plagioclase), Sil (sillimanite), St_c, St_n, St_r, and St_{ro}. (staurolite, with subscripts defined as described above).

the path are recorded in rocks from the upper horizon of the schist of Stevens Spring and the second two segments are recorded in rocks from the lower horizon. Garnet in the two horizons record different parts of the PT path due to different garnet growth reactions. The PT paths record two burial events separated by ~3 kbar of decompression. The first burial episode records a 2 kbar pressure increase at ~515–550°C; the second burial episode records ~1 kbar of pressure increase at ~585°C to 615°C.

3.2. Dating the "M-Shaped" PT Path

3.2.1. Dating of Older (UH) Garnets by Lu-Hf Garnet Geochronology

[18] In this study we report an age determined using the Lu-Hf method [e.g., *Anczkiewicz et al.*, 2007; *Cheng et al.*, 2008] on the older (upper horizon) garnets from which detailed PT paths have been determined (Figures 4a and 5a). Details of sample preparation and analytical procedures are presented in Appendix A. Six 200–250 mg fractions of visually clear garnet and ~250 mg of bulk rock were selected for isotopic analysis. All data (6 garnet fractions and 1 whole rock) taken together yield an age of 85.4 ± 2.2 Ma with an initial $^{176}Hf/^{177}Hf$ of 0.28245 ± 5 ($\varepsilon_{Hf} = -10.0 \pm 1.9$) but with a somewhat elevated MSWD (5.6). Elimination of one of the garnet points (G5) yields an identical age of 85.5 ± 1.9 (initial $^{176}Hf/^{177}Hf$ = 0.28244 ± 5; $\varepsilon_{Hf} = -10.3 \pm 1.8$) but with slightly smaller error and lower MSWD (3.9) (Figure 6). The whole rock point plots below the isochron and is contributing to the higher MSWD. This is commonly observed in garnet whole-rock isochrons if inherited zircons are present in the rock [*Scherer et al.*, 2000] because they are contributing less radiogenic Hf to the whole-rock composition. Regression of only the garnet points yields an age of 84.5 ± 1.8 that is within error of the garnet whole-rock isochron but with a lower MSWD (2.3). This MSWD, while above 1, is still quite low considering the small uncertainties of the data points and the large spread in Lu/Hf of the individual points. Model ages were determined for each garnet fraction using the $^{176}Hf/^{177}Hf$ and $^{176}Lu/^{177}Hf$ ratios for the garnet fraction combined with the calculated initial $^{176}Hf/^{177}Hf$ and $^{176}Lu/^{177}Hf$ ratios from the regression using all data. Model ages for the garnet fractions are 85.3 ± 1.5 (G1), 87.5 ± 2.7 (G2), 87.5 ± 2.9 (G3), 86.5 ± 3.1 (G4), 88.8 ± 2.2 (G5) and 85.34 ± 0.81 Ma (G6) (Table 2 and Figure 6). Model ages produce weighted means of 85.8 ± 1.3 Ma (MSWD = 2.5, all garnets) and 85.6 ± 0.6 Ma (MSWD = 1.2, omitting garnet 5).

[19] Collectively, these data define a robust Lu-Hf garnet age of about 86 Ma. This age is interpreted to record the timing of prograde garnet growth based on the observations that garnet growth occurred under temperature conditions of ~515–550°C and that subsequent metamorphic temperatures peaked at ~630°C (Figures 4), well below the nominal closure temperature for the Lu-Hf system in garnet of 900°C [*Anczkiewicz et al.*, 2007]. The PT paths for the older (upper horizon) garnets (Figures 4a and 4c) indicate that garnet grew during ~2 kbar of pressure increase (~7.5 km of burial). Therefore, our interpretation is that a significant thrust burial event is documented at ~86 Ma. This constrains the age of post-thrusting exhumation to the interval 86–65 Ma, bracketed between the 86 Ma Lu-Hf age for

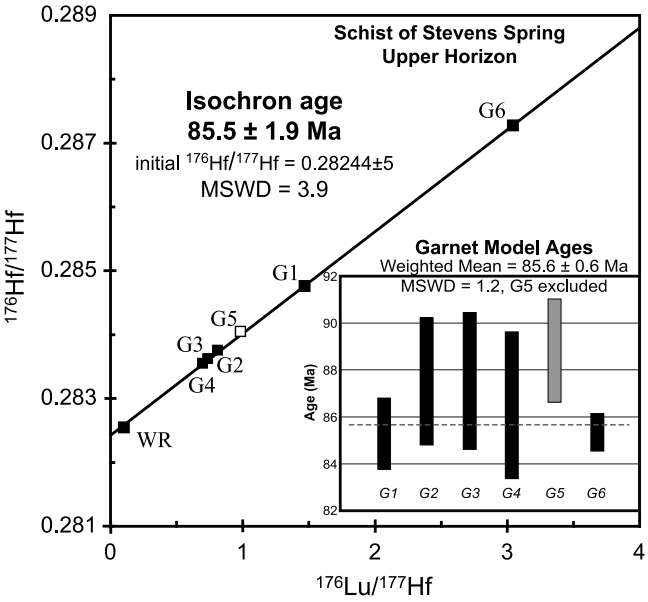

Figure 6. Lu-Hf isochron for sample UH2. G, garnet; WR, whole rock. Data in Table 2. Exclusion of the whole rock point in the isochron calculation yields an age of 84.5 ± 1.8 (MSWD = 2.3) for a garnet-only regression. The symbols are much larger than the 2σ uncertainties for the data points (0.01% for $^{176}Hf/^{177}Hf$ and 0.5% for $^{176}Lu/^{177}Hf$) and would be too small to show on this diagram. See text for details.

upper horizon garnets and the oldest garnet core model age (65 Ma) determined from monazite inclusions by *Hoisch et al.* [2008] for the lower horizon garnets (see below).

3.2.2. Dating of Younger (LH) Garnets by Th-Pb Dating of Monazite Inclusions

[20] Dating of the younger (lower horizon) garnets was previously carried out by inferring the age of garnet growth from a population of very small (<20 μm) monazite inclusions in garnet. Ages from sixty-six monazite inclusions in four large (~1 cm) garnet grains analyzed in situ were reported by *Hoisch et al.* [2008]. In all four garnet grains, monazite ages decrease with radial distance from the garnet cores. *Hoisch et al.* [2008] constructed "model" ages for the garnet cores and rims (Figure 7a), based on the assumptions that (1) garnet growth occurred with a constant rate of volume increase, (2) monazite inclusions co-crystallized with garnet at the garnet rims and were occluded as the garnet grew, and (3) monazite grains, once occluded, were armored from further changes such as Pb loss, dissolution or new growth, as suggested in many studies [e.g., *DeWolf et al.*, 1993; *Poitrasson et al.*, 1996; *Zhu et al.*, 1997; *Braun et al.*, 1998; *Foster et al.*, 2000; *Montel et al.*, 2000; *Simpson et al.*, 2000; *Stern and Berman*, 2001; *Terry et al.*, 2000]. In addition, temperatures remained well below the >900°C threshold for Pb diffusion in monazite [e.g., *Cherniak et al.*, 2004]. From the regressions, model ages for the garnet cores and rims were calculated. Model ages for garnet cores range from 56.9 ± 5.6 to 64.4 ± 5.0 Ma (Figure 7b). Model ages for the garnet rims vary more widely, due to variable amounts of retrograde rim consumption; however, the largest difference between the model ages of the core and rim found on any one garnet grain was 22 m.y. (Figure 7b). Thus, using the oldest core model age, the age of the second garnet growth event and associated burial is constrained to 65–45 Ma, and garnet growth during burial may have begun prior to 65 Ma.

[21] From the same rocks, *Strickland et al.* [2011a] determined ages on monazite grains that were separated from crushed whole rock by heavy liquids. We consider it unlikely, however, that the very small (<20 μm) garnet-hosted monazite inclusions were successfully separated by this process, as evidenced by the similarity of the age population they determined (38–53 Ma based on 10 U-Pb determinations) with the matrix age population reported by *Hoisch et al.* [2008] (25–58 Ma based on 30 Th-Pb determinations). *Strickland et al.* [2011a] regressed intercept ages of 39.5 ± 4.2 and 2236 ± 450 Ma from five of their data points, suggesting partial Pb-loss at 39.5 Ma. They interpreted the other five fractions to represent either continuous recrystallization of monazite from 53 to 38 Ma, or partial resetting of older grains during Eocene or younger metamorphism. Recrystallization of monazite is consistent with the interpretation of *Hoisch et al.* [2008], who proposed that the matrix grains underwent fluid mediated partial dissolution, reprecipitation and variable resetting, possibly associated with the intrusion of the 27–29 Ma Vipont pluton (ages for phases of the Vipont pluton have been reported by

Table 2. Lu-Hf Isotope Data for the Pelitic "Upper Horizon" of the Schist of Stevens Spring, Basin Creek, Grouse Creek Mountains

Sample	Lu[a] (p.p.m.)	Hf[a] (p.p.m.)	$^{176}Lu/^{177}Hf$[b]	$^{176}Hf/^{177}Hf$[c]	Plus or Minus[d]	Model Ages[e] (Ma)	Error in Age (2σ)
G1	9.68	0.938	1.465	0.284774	6	85.3	1.5
G2	7.90	1.39	0.8057	0.283758	5	87.5	2.7
G3	7.73	1.50	0.7311	0.283636	6	87.5	2.9
G4	6.92	1.42	0.6935	0.283561	6	86.5	3.1
G5	10.5	1.53	0.9788	0.284064	4	88.8	2.2
G6	8.70	0.407	3.039	0.287286	6	85.3	0.8
WR	0.506	0.743	0.09664	0.282558	3		

[a]Lu and Hf concentrations determined by isotope dilution with uncertainties estimated to be better than 0.5%.
[b]Uncertainties for $^{176}Lu/^{177}Hf$ for the purpose of regressions and age calculations is estimated to be 0.5%.
[c]The $^{176}Hf/^{177}Hf$ ratios were corrected for instrumental mass bias using $^{179}Hf/^{177}Hf = 0.7935$ and normalized relative to $^{176}Hf/^{177}Hf = 0.282160$ for JMC-475 [*Vervoort and Blichert-Toft*, 1999]. Epsilon Hf values calculated with Lu-Hf CHUR values of *Bouvier et al.* [2008] and the ^{176}Lu decay constant value of *Scherer et al.* [2001] and *Söderlund et al.* [2004].
[d]Reported errors on $^{176}Hf/^{177}Hf$ represent within-run uncertainty expressed as 2σ, standard error. Uncertainty is given as variation in the 6th place. Estimated total uncertainty on individual $^{176}Hf/^{177}Hf$ measurements for the purpose of regressions and age calculations is estimated to be 0.01% or about 1 ε_{Hf} unit.
[e]Model ages reported for each garnet fraction using the $^{176}Hf/^{177}Hf$ and $^{176}Lu/^{177}Hf$ ratios for the garnet fraction combined with the calculated initial $^{176}Hf/^{177}Hf$ and $^{176}Lu/^{177}Hf$ ratios from the regression using all data.

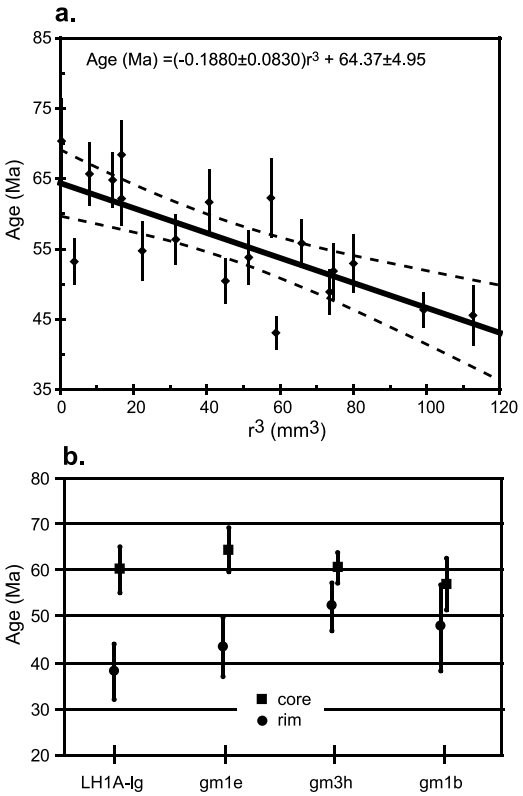

Figure 7. (a) Plot of Th-Pb ages of monazite inclusions in garnet gm1e versus radial distance cubed from garnet core [*Hoisch et al.*, 2008]. One-sigma error bars are shown on data points; error envelope for the 95% confidence interval is shown. (b) Calculated core and rim garnet "model ages" calculated by the regression of inclusion ages versus radial distance cubed. Error bar shown is 95% confidence interval.

Compton et al. [1977], *Wells et al.* [1997], and *Strickland et al.* [2011a, 2011b]).

[22] From the Basin Creek area, *Strickland et al.* [2011a] also reported 27 monazite U-Pb ages ranging from 27 to 33 Ma from the Archean Greek Creek complex, and 34 monazite ages from a garnet-absent sample of the schist of Stevens Spring. The latter include monazite cores that averaged 140.7 ± 1.5 Ma (n = 9) and 25 determinations of rims and whole grains with patchy zonation that ranged from 35.5 to 30.0 Ma [*Strickland et al.*, 2011a]. In addition, *Strickland et al.* [2011a] analyzed detrital cores and metamorphic rims on zircons, from the same garnet-absent sample of the schist of Stevens Spring. Sixty-eight age determinations on cores ranged from 2757 ± 10 to 899 ± 65 Ma, while 23 determinations on rims were discordant and ranged in age from 146 ± 1 to 110 ± 1 Ma.

[23] *Strickland et al.* [2011a] interpreted the sillimanite in these rocks to be related to contact metamorphism from the 27–29 Ma Vipont granite, based on an analogy with sillimanite in the contact aureoles of other Tertiary granitic bodies in the Grouse Creek and Albion Ranges, and on the similarity of zircon rim ages and some monazite ages obtained from metamorphic rocks in Basin Creek with the age of the Vipont granite (discussed earlier). We concur that sillimanite was stable during the inception of shearing along the Middle Mountain shear zone, but disagree with the interpretation of a contact metamorphic origin for sillimanite at Basin Creek. The other known occurrences of sillimanite are found along the immediate contacts (within tens of meters) of sizable contiguous granitic bodies (the Almo pluton in the Albion Range, the Red Butte stocks in the Grouse Creek Range, and the Vipont pluton further north), whereas in the Basin Creek area, the Vipont granite occurs as sparse dikes occupying only 1–3% of the total rock volume. The proportion of granite increases northward from Basin Creek, and 8 km north of Basin Creek the sill-like Vipont pluton has a minimum thickness of 300 m, with an additional 100–150 m thick lit-par-lit injection zone present in its roof. Contact-metamorphic sillimanite at this locality is present in screens of staurolite-absent pelitic schist within the injection zone. We interpret the full set of geochronologic data to record essentially continuous metamorphism that began prior to ~140 Ma, peaked at about 40 Ma, and ended upon falling below the closure temperature for argon diffusion in biotite at 21 Ma [*Wells et al.*, 1997], rather than two separate episodes of metamorphism at ~140 Ma and ~30 Ma, as interpreted by *Strickland et al.* [2011b].

3.3. Structural Evidence for Kinematic Alternations

[24] Multiple cycles of shortening and extension from Late Jurassic to Late Eocene time have previously been recognized in the RAG MCC (Table 1 and Figure 2). The principal field observations that document the Late Cretaceous to Eocene kinematic alternations are summarized below. Low-angle faults that omit parts of the stratigraphic section and lie structurally above the schist of Stevens Spring have previously been described and interpreted as Late Cretaceous normal faults [*Wells*, 1997; *Wells et al.*, 1998] (D2, Table 1), including the Mahogany Peaks and the Emigrant Spring faults. The Mahogany Peaks fault places Ordovician rocks over Neoproterozoic rocks (Figure 3), removes about 4 km of strata and has an estimated slip of >20 km. Juxtaposition of younger over older rocks, and of upper greenschist-facies metamorphic rocks yielding 90 Ma muscovite $^{40}Ar/^{39}Ar$ cooling ages over middle amphibolite-facies metamorphic rocks yielding 60 Ma muscovite $^{40}Ar/^{39}Ar$ cooling ages, as well as top-to-the-west shearing down-structure, support an extensional origin for this fault. The Emigrant Spring fault (Figure 3) places Pennsylvanian over Ordovician marble, removes about 5 km of stratigraphy, and also exhibits top-to-the-west kinematics. Both faults deform a mid-Cretaceous fabric and are deformed by recumbent folds, which are in turn overprinted by an Eocene detachment fault and shear zone.

[25] The previous interpretation of alternations in shortening and extension relied on the interpretation that recumbent folds, which deform the Late Cretaceous low-angle normal faults, represent renewed shortening [*Wells*, 1997]. Recumbent folds can form during extension, however, such occurrences are usually associated with high-strain rock fabrics including mylonite and sheath folds [e.g., *Cobbold and Quinquis*, 1980; *Malavieille*, 1987] or alternatively, an initial moderate to steep dip to layering [e.g., *Froitzheim*, 1992]. The folds that deform the Mahogany Peaks and Emigrant Spring faults lack coeval high-strain features, and there is no evidence for a significant regional dip to the bedding-parallel faults. Thus, it seems improbable that the

folds developed during horizontal extension and vertical shortening.

[26] Recumbently folded low-angle normal faults and shear zones have been interpreted to record a return to shortening following a period of extension at mid-crustal levels [e.g., *Balanyá et al.*, 1997; *Beltrando et al.*, 2008]. The folding of the low-angle faults in the RAG MCC may be related to renewed thrust motion along the Basin-Elba fault. At Mt. Harrison in the Albion Mountains, the Mahogany Peaks fault is folded into an east-vergent, tight to isoclinal syncline in the footwall of the Basin-Elba fault [*Miller*, 1980, 1983], suggesting a kinematic association between folding and thrusting.

[27] A return to extension is manifest in the development of an Eocene extensional shear zone-detachment fault system, the Middle Mountain shear zone and associated Middle detachment fault, which overprint the tight to recumbent folds (D4a, Table 1) [*Wells et al.*, 2000]. Existing geo- and thermo-chronometry suggests that the first phase of top-to-the-NW ductile shearing along the Middle Mountain shear zone predates intrusion of Oligocene (29–25 Ma) granites and was initiated by 45 Ma, as indicated by $^{40}Ar/^{39}Ar$ cooling ages in its footwall [*Wells et al.*, 2000]. Eocene extension in the RAG MCC fits well with the documented southward sweep in the onset of extension [e.g., *Axen et al.*, 1993; *Dickinson*, 2002], and closely followed the termination of shortening.

4. Geodynamic Model

[28] The kinematics of deformation in orogenic belts are governed by the dynamic interplay between many factors including gravitational potential energy, plate boundary forces, rock rheology and erosion [*Davis et al.*, 1983; *Platt*, 1986; *Molnar and Lyon-Caen*, 1988; *England and Houseman*, 1989]. A change from shortening to extension during active plate convergence may be triggered by a decrease in horizontal compressive stress, increase in gravitational potential energy, or reduction in rock strength [*Platt*, 1986; *England and Houseman*, 1989; *Willett*, 1992; *Rey et al.*, 2001] (Figure 9). The converse is also true, that renewed shortening in the rear of an orogenic wedge may be triggered by an increase in horizontal compressive stress, decrease in gravitational potential energy, an increase in rock strength, or factors that lead to a decrease in orogenic taper (i.e., erosion, frontal offscraping). Here we address the geodynamic conditions responsible for the transitions in deformation kinematics implied by the "M-shaped" PTt path from the Grouse Creek Mountains.

4.1. Late Cretaceous Transition From Shortening to Extension

[29] Late Cretaceous extension, documented by the Mahogany Peaks fault and the PTt path presented here from the RAG MCC, appears to have been widespread in the hinterland of the Sevier-Laramide orogen [*Wells and Hoisch*, 2008, and references therein]. Evidence for this is more abundant in the Mojave sector of SE California, above the purported shallowly dipping to flat segment in the subducted Farallon slab, however, scattered examples north of the inferred slab-segment boundary of *Saleeby* [2003] within the hinterland of the Idaho-Utah-Wyoming sector suggest that both regions experienced similar processes.

[30] The most common geodynamic environment for synconvergent extension is slab rollback and its associated reduction in plate coupling [*Royden*, 1993; *Rawling and Lister*, 1999; *Collins*, 2002; *Beltrando et al.*, 2007; *Jolivet and Brun*, 2010] (Figure 8a). Slab rollback occurs when the rate of plate convergence is less than the rate of subduction, the latter of which is controlled largely by the negative buoyancy of the subducting slab [e.g., *Royden*, 1993]. Slab rollback reduces the coupling at the plate boundary, thus lessening the resulting horizontal compressive stress. Additionally, enhanced counterflow in the mantle wedge, modified by slab rollback, provides traction at the base of the overriding lithosphere, and induces uplift due to dynamic topography, which both further promotes extension [e.g., *Humphreys*, 1995].

[31] The dip of the subducting Farallon plate is thought to have shallowed, rather than steepened, beneath the western North America during the Late Cretaceous, as indicated by reconstructed plate motions [*Engebretson et al.*, 1985; *Müller et al.*, 1997], inverse modeling of mantle convection [*Liu et al.*, 2008, 2010], and the geology of the overriding plate [e.g., *Coney and Reynolds*, 1977; *Bird*, 1984; *Liu and Nummedal*, 2004]. Slab rollback is thus not a viable mechanism for Late Cretaceous synconvergent extension of the Sevier orogen. A variant of slab rollback in which "pinned" slab rollback occurs at the trailing edge of a subducted oceanic plateau, at the transition to abyssal lithosphere (Figure 8b), has been proposed as a geodynamic mechanism for Late Cretaceous extension in the Mojave Desert region [*Saleeby*, 2003]. This mechanism was discounted by *Wells and Hoisch* [2008] based on the chemical and thermal contribution of basalts to anatectic melts, and the occurrence of anatexis and extension on either side of the northern margin of the subducted oceanic plateau [*Saleeby*, 2003; *Liu et al.*, 2010]. In the absence of slab rollback, three mechanisms for Late Cretaceous synconvergent extension are seemingly compatible with the geologic observations from the hinterland of the Late Cretaceous Sevier-Laramide orogen (Figure 8) (see *Wells and Hoisch* [2008] for a more complete discussion): rheological weakening, focused internal shortening, and delamination. These mechanisms are not mutually exclusive, and may, indeed, be related to one another.

[32] A reduction in the strength of material within an orogenic wedge or its basal decollement can induce extension (Figure 8c). Weakening of the basal décollement, without a similar weakening of the material within the wedge, in Coulomb-plastic and viscous wedges [*Dahlen*, 1984; *Willett*, 1992, 1999], accomplishes a reduction in basal shear stress that can lead to horizontal extension. Furthermore, weakening of material within a viscous wedge will result in a decrease in the critical taper and extension [*Willett*, 1999; *Rossetti et al.*, 2002]. Similarly, weakening of the mid- to lower-crust may lead to decoupling, allowing the crust to flow in response to lateral gradients in gravitational potential energy [*Jamieson et al.*, 1998; *Vanderhaeghe and Teyssier*, 2001] (Figure 8d). Heating, to facilitate rheological weakening, may occur more gradually through thermal relaxation of tectonically thickened crust [e.g., *England and Thompson*, 1984] or more rapidly through heat advection by invasion of basaltic melts [e.g., *Annen and Sparks*, 2002]. Upon heating, weakening is predicted by the temperature sensitivity of plastic flow laws [*Kohlstedt et al.*, 1995] and

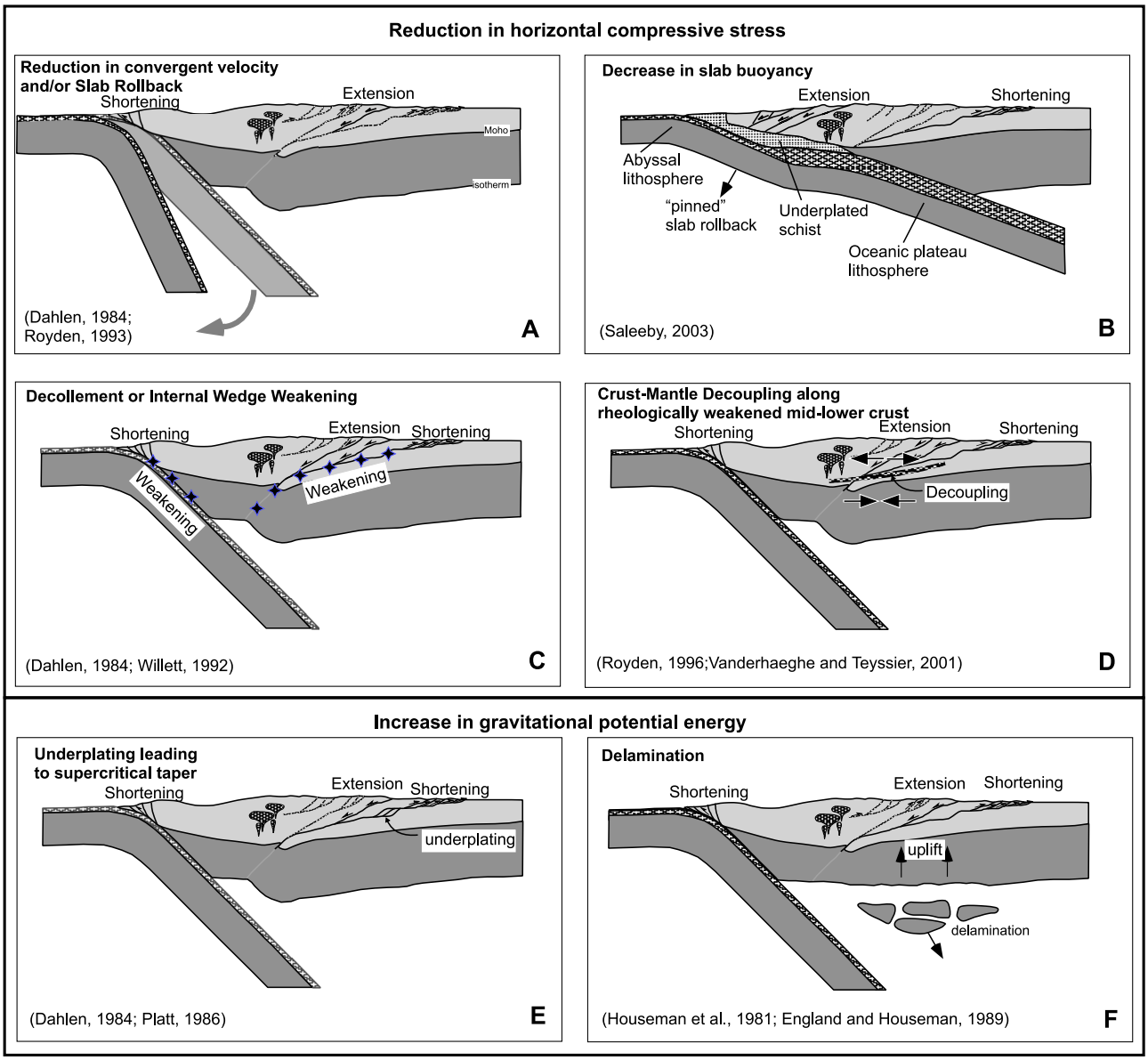

Figure 8. (a–f) Tectonic cartoons illustrating various factors that may trigger synconvergent extension. Note that (left) oceanic and (right) continental lithosphere are converging in all cases. See text for discussion. Note that these internal and external factors may operate in isolation or in various combinations within particular tectonic settings of synconvergent extension.

— should partial melting occur — by melt-induced weakening mechanisms [*Jamieson et al.*, 1998; *Handy et al.*, 2001]. The production of Cordilleran-type peraluminous granites [*Barton*, 1990; *Patiño Douce*, 1999] in the Sevier hinterland was probably associated with rheological weakening at the melt sites in the lower crust.

[33] Focused internal shortening in the rear of an orogenic wedge may also trigger extension by over-steepening its taper to a supercritical state [*Dahlen*, 1984; *Platt*, 1986; *Cello and Mazzoli*, 1996] (Figure 8e). Thickening may occur by underplating at the base of the wedge or by internal shortening within the wedge [e.g., *Platt*, 1986]. Duplex faulting and development of antiformal culminations are efficient in localizing crustal thickening, causing topographic uplift, and increasing wedge taper [*DeCelles and Mitra*, 1995], and are commonly associated with crustal ramps. Several MCCs of the Sevier orogen, including the RAG MCC, are paired with regional synclinoria on their east sides, suggesting uplift over crustal-scale ramps [e.g., *Armstrong*, 1982; *Von Tish et al.*, 1985]. The ramps may have undergone footwall imbrication to form large duplexes, similar to the culminations related to steps in the basement further east [e.g., *Yonkee*, 1992; *DeCelles et al.*, 1995]. It is unclear whether extension above a zone of duplexing at the base of the Sevier orogenic wedge would be of sufficient magnitude and rate to produce ~3 kbar of decompression without cooling. Additionally, while extension above duplexes associated with large-scale ramps may seem reasonable for individual core complexes, application of this mechanism to all documented localities of Late Cretaceous extension from

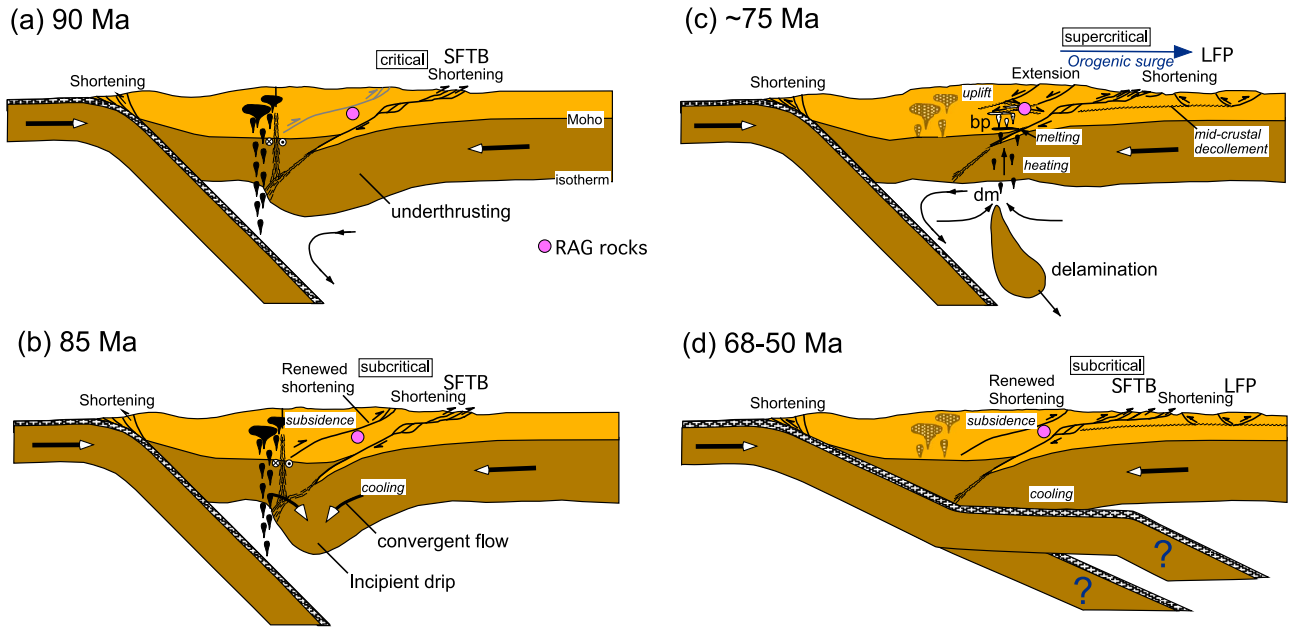

Figure 9. Proposed tectonic model for the Late Cretaceous to early Eocene evolution of the Sevier-Laramide orogen. (a) Development of thick lithospheric root during plate convergence. Mass balance requires an equivalent magnitude of shortening of mantle lithosphere as shortening of crust. (b) Thickened lithospheric root becomes gravitationally unstable and weak part of root flows inward and downward (convergent flow) into incipient drip. Convergent flow in mantle causes isostatic subsidence, cooling, and renewed shortening in crust, compounded by coupled convergent flow in crust. (c) Separation of mantle drip from continental lithosphere produces isostatic uplift, basaltic decompression melts (dm) of asthenosphere that pond (bp) in lower crust, and heating and anatexis. Isostatic uplift shifts orogenic wedge into supercritical state, triggering hinterland extension, lengthening of wedge by propagation of décollement into Laramide foreland province. (d) Lower angle subduction during accelerated westward drift of North America and North America-Farallon plate convergence leads to increased plate coupling, cooling of North American lithosphere, subsidence, subcritical orogenic taper, and renewed shortening in hinterland. RAG, Raft River-Albion-Grouse Creek; SFTB, Sevier fold-thrust belt; LFP, Laramide foreland province. Inactive faults and magmatism shown in gray.

southeastern California to Idaho-Montana is unlikely. The >2 kbar pressure increase immediately preceding decompression requires tectonic burial of the RAG MCC rocks themselves, and suggests that underplating by itself is not a viable explanation. The MCCs lay within, rather than beneath, the Sevier orogenic wedge and a western thrust internal to the wedge is required to bury the RAG MCC [e.g., *Camilleri et al.*, 1997; *Harris et al.*, 2007]. Furthermore, there is abundant evidence for localized crustal thickening in the metamorphic rocks of MCCs, in the form of depth-controlled metamorphic field gradients [*Hoisch and Simpson*, 1993; *Camilleri and Chamberlain*, 1997; *Lewis et al.*, 1999; *McGrew et al.*, 2000; *Cooper et al.*, 2010]. The viability of thickening internal to the orogenic wedge as a mechanism for triggering extension is discussed below in reference to the PTt path.

[34] It is well recognized that delamination of mantle lithosphere (Figure 8f) is an effective mechanism to increase Moho temperature and geothermal gradient, induce adiabatic asthenospheric melting, increase gravitational potential energy, increase elevation, and trigger crustal extension [*Houseman et al.*, 1981; *Platt and England*, 1994; *Rey et al.*, 2001]. Additionally, the delamination cycle and its associated thermal and isostatic responses may significantly alter the dynamics of orogenic wedges, and not only lead to extension, but promote focused shortening as an antecedent to delamination. By delamination cycle, we refer to the phases of development and amplification of a Rayleigh-Taylor (RT) instability, separation (delamination), and post-separation thermal, isostatic, and rheological re-equilibration.

[35] Numerical modeling suggests the following sequence for the development and foundering of gravitationally unstable thickened mantle lithosphere [e.g., *Molnar et al.*, 1998; *Conrad and Molnar*, 1999; *Conrad*, 2000]: (1) initial thickening of mantle lithosphere developing a RT instability; (2) increase in the amplitude of the RT instability by convergent flow; (3) transition from linear viscous flow (diffusion creep) and exponential growth of the developing instability to power law flow (dislocation creep) and super-exponential growth and; (4) detachment and sinking of the RT instability (mantle drip).

[36] Uplift and the change in the taper of orogenic wedges to supercritical are predicted to accompany detachment and sinking of mantle lithosphere beneath the rear of retroarc wedges. The consequences of isostatic uplift and the rotation in maximum principal compressive stress from horizontal to vertical immediately following the separation of convectively unstable lithospheric roots are well recognized [e.g.,

Molnar and Lyon-Caen, 1988; *Houseman and Molnar*, 1997; *Rey et al.*, 2001]. Lateral gradients in gravitational potential energy sufficient to cause extension are derived from both topographically elevated crust (relative to lowlands) as well as from thickened mantle lithosphere [*Rey et al.*, 2001]. The accompanying increase in Moho temperature and geothermal gradient, and heat advection due to invasion by adiabatic asthenospheric melts induced by delamination, also promote extension. Delamination beneath the rear of retroarc orogenic wedges is predicted due to the inherent asymmetry in the locus of crustal and lithospheric mantle thickening in the retroarc, and the proximity to the arc wherein dense eclogite facies garnet pyroxenites, residues of melting, may also participate in and promote delamination [e.g., *Ducea*, 2002]. The increase in taper of the orogenic wedge leads to extension in its rear and lengthening at its toe, providing a kinematic link between hinterland extension and foreland shortening.

[37] We have previously proposed that delamination is the likely cause for Late Cretaceous extension in the Sevier-Laramide orogen based upon petrologic, structural, and thermochronologic data [*Wells et al.*, 2005; *Wells and Hoisch*, 2008]. Salient observations include: similar timing of Late Cretaceous extension, with up to 14 km of exhumation, from multiple localities along the axis of prior crustal thickening; association in space and time of extension with Late Cretaceous Cordilleran-type peraluminous granites, which have a deep crustal source but also a juvenile basaltic component; and extension and magmatism synchronous with continued shortening in both the Laramide foreland province and the Sevier fold-thrust belt northeast of the Mojave Desert. Additionally, the PT path departed significantly from paths of Barrovian metamorphism [e.g., *England and Thompson*, 1984], and requires a heat source external to the crust. The proposal of Late Cretaceous delamination at the onset of the Laramide orogeny [*Wells and Hoisch*, 2008] relies on observations of the geologic consequences of delamination and the elimination of competing models.

[38] The new Lu-Hf garnet ages presented here, coupled with the Th-Pb monazite inclusion ages [*Hoisch et al.*, 2008] and revised PT paths [*Hoisch et al.*, 2002; *Harris et al.*, 2007], allow us to better test the alternative mechanisms of rheological weakening, focused internal shortening, and delamination for Late Cretaceous synconvergent extension in the hinterland of the Idaho-Utah-Wyoming sector, as each makes testable predictions of PTt paths. In the case of rheological weakening through thermal relaxation of tectonically thickened crust, rocks undergo clockwise PT paths characterized by a significant time lag between peak pressure and temperature [e.g., *England and Thompson*, 1984], with isobaric heating and or heating with limited decompression following shortening-related compression. Exhumation triggered by rheological weakening will be close in timing to peak temperature conditions in the lower crust. In contrast, extension triggered solely by supercritical wedge formation should produce a PT path lacking a period of isobaric heating following compression and exhibit decompression closely following compression. Cooling will accompany decompression unless the rate of decompression is slow relative to the rate of radiogenic heat production. Finally, delamination of mantle lithosphere may produce either heating during decompression or isobaric heating following decompression [*Platt and England*, 1994], depending on the rate of exhumation.

[39] The PTt path presented here for the Late Cretaceous to early Eocene tectonics of the Grouse Creek Mountains is most supportive of delamination of mantle lithosphere as a driving mechanism for the Late Cretaceous tectonic mode switch from shortening to extension (Figure 9c). Decompression is bracketed between the two dated garnet growth events of 86 and 65 Ma. Muscovite cooling ages from the hanging wall and footwall of the Mahogany Peaks fault in the eastern Raft River Mountains of 90 and 60 Ma, respectively, are compatible with exhumation of the schist of Stevens Spring by the Mahogany Peaks and Emigrant Spring faults [*Wells et al.*, 1998]. The apparently continuous heating during a sequence of compression-decompression-compression is inconsistent with oversteepening of an orogenic wedge, whether by underplating or internal thickening, as being the sole driver for extension. Furthermore, continued heating following decompression is inconsistent with rheologic weakening as the principal driving mechanism for extension. Delamination and associated heating of the crust through an increase in Moho temperature and mantle heat flux, perhaps enhanced by intrusion of decompression-related asthenospheric melts into the lower crust [*Annen and Sparks*, 2002], seems necessary to explain the inferred heating during exhumation in this area (Figure 9c). We note that while 85–70 Ma plutons are present elsewhere in the Sevier hinterland [e.g., *Barton*, 1990; *Wright and Wooden*, 1991], there are no exposed plutons of this age in the nearby region. Thus, while focused crustal thickening, and perhaps rheological weakening, aided in localizing and promoting Late Cretaceous extension, we view delamination to be the fundamental cause.

[40] Delamination provides a context for viewing the significant 86 Ma crustal thickening (minimally 7 km) in the interior of the orogenic wedge that predated Late Cretaceous decompression. The delamination cycle predicts subsidence to precede delamination. Flexural isostatic subsidence accompanying growth and amplification of an RT instability may lower orogenic taper and lead to renewed shortening in the interior of the wedge. Subsidence may be rapid due to the predicted acceleration of downwelling during growth of the RT instability [*Conrad*, 2000]. Shortening required by orogenic wedge mechanics would be reinforced by kinematically and rheologically required convergent flow associated with downwelling during the growth of a RT instability (Figure 9b). The areal extent of such shortening would scale with the diameter of the RT instability.

[41] Late Cretaceous shortening and metamorphism that immediately preceded extension, as documented in the RAG MCC, is evident elsewhere in the MCCs of the Sevier hinterland, and is superimposed on Late Jurassic to Early Cretaceous metamorphism associated with folding and foliation development [*Miller et al.*, 1988; *Hudec*, 1992, *Camilleri and Chamberlain*, 1997; *McGrew et al.*, 2000; *Cruz-Uribe et al.*, 2008; *Cooper et al.*, 2010]. In the Snake Range MCC, garnet growth associated with burial of Neoproterozoic supracrustal rocks to metamorphic pressures of up to 8 kbar has been dated by Sm-Nd and Lu-Hf garnet isochrons as Late Cretaceous (88.8 ± 1.2 and 90.8 ± 1.8 Ma, respectively [*Cooper et al.*, 2010]), consistent with prior constraints on the age of Late Cretaceous metamorphism [*Miller*

et al., 1988]. In the Ruby Mountains-East Humboldt Range MCC, peak metamorphic pressures of 9 kbar were reached at ~85 Ma [*McGrew et al.*, 2000], consistent with an 84.1 ± 0.2 Ma age for peak metamorphism (U-Pb, metamorphic sphene) in the adjacent Pequop Mountains [*Camilleri and Chamberlain*, 1997]. A post-metamorphic period of thrusting is bracketed between 84 and 75 Ma in the Wood Hills [*Camilleri and Chamberlain*, 1997]. The distinction between Late Jurassic and Late Cretaceous metamorphism in the Funeral Mountains MCC is less clear; however, a Th-Pb age of 91.5 ± 1.4 Ma reported by *Mattinson et al.* [2007] on monazite from garnet-staurolite-kyanite schist that records peak metamorphism at 7–9 kbars [*Labotka*, 1980; *Hoisch and Simpson*, 1993], leaves open the possibility that shortening continued into the Late Cretaceous.

[42] It is well recognized that the MMCs of the Sevier hinterland exhibit evidence for localized large magnitude crustal thickening and burial [e.g., *Armstrong*, 1982; *Coney and Harms*, 1984]. Thickening and burial was not uniform along strike, as evident in the significant lateral metamorphic field gradients in contiguous metamorphic rocks (up to 4–6 kbar differences in pressure over lateral distances of 30 to 40 km) as seen in the Funeral Mountains [*Labotka*, 1980; *Hoisch and Simpson*, 1993], Snake Range [*Miller et al.*, *1988*; *Lewis et al.*, 1999; *Cooper et al.*, 2010], and Ruby Mountains-East Humboldt Range [*Howard*, 2003, and references therein]. The patchy distribution of metamorphic rocks of appropriate mineralogy for thermobarometry in the RAG MCC, as well as the variability in age of Mesozoic metamorphism being revealed by ongoing work [e.g., *Cruz-Uribe et al.*, 2008; *Strickland et al.*, 2011a], has not allowed lateral variations in Late Cretaceous metamorphic conditions to be evaluated; however, existing constraints do not preclude such lateral variations. Any explanation for the development of the metamorphic field gradients must account for a significant variability in burial parallel to the orogen [e.g., *Howard*, 2003; *Cooper et al.*, 2010].

[43] The metamorphic field gradients may represent focused crustal thickening and differential burial associated with duplexes at major crustal ramps [e.g., *Miller and Hoisch*, 1995; *Camilleri*, 1998; *Wells et al.*, 2008]. Tectonic burial may have been focused at basement buttresses (walls and corners) related to the geometry of the Late Precambrian rift system and its consequent Paleozoic shelf-slope break [*Miller et al.*, 1991; *Wells et al.*, 2008]. However, it is permissive that the pronounced metamorphic field gradients may in part record localized downwelling as a manifestation of convergent flow over a RT instability. Localized subsidence and basin formation on the Puna plateau of the Andes has recently been proposed as a surface manifestation of such downwellings [*Carrapa et al.*, 2009].

4.2. Extension to Shortening Transition: Renewed Late Cretaceous to Eocene Shortening

[44] During the Late Cretaceous to Early Eocene, a marked increase in the rate of shortening across the foreland of the Sevier-Laramide orogen is recorded by coeval shortening in the Sevier fold-thrust belt and to the east, in the Laramide foreland province [*Dickinson et al.*, 1988; *DeCelles*, 2004, Figure 4b] (Figure 2). Early in this time interval, the hinterland region experienced partial melting, extension, and exhumation [*Hodges and Walker*, 1992; *Camilleri and Chamberlain*, 1997; *McGrew et al.*, 2000; *Wells and Hoisch*, 2008] (Figure 9c). We infer that these processes are in response to delamination, and thus also predict uplift. Uplift will result in supercritical taper, and consequent extension in the hinterland may have been kinematically linked to foreland shortening [cf., *Livaccari*, 1991]. Thus, uplift and extension in the hinterland may have caused propagation of deformation into the Laramide foreland, akin to an orogenic surge [e.g., *Lister et al.*, 2001], effectively lengthening the orogenic wedge and lowering the taper (Figure 9c).

[45] Following lithospheric foundering, anatexis and extension in the hinterland, an increase in net horizontal compressive stress in the hinterland is predicted from: (1) relaxation of contrasts in gravitational potential energy and associated horizontal tensional stresses; (2) an increase in plate coupling due to an increase in relative convergence rate between the Farallon and North American plates [*Engebretson et al.*, 1985] and an increase in surface area of plate contact, whether by end loading or basal shear [*Bird*, 1984; *Livaccari and Perry*, 1993], perhaps amplified by subduction of an aseismic ridge or oceanic plateau [*Henderson et al.*, 1984; *Barth and Schneiderman*, 1996]. Upon cooling, continuity of the continental stress guide is restored, and with increased subhorizontal compression and thermal subsidence on the heels of extension-related mechanical subsidence [e.g., *McKenzie*, 1978], shortening is renewed in the hinterland and critical taper to the orogenic wedge is reestablished (Figure 9d). Renewed shortening in the hinterland of the Sevier fold-thrust belt, recorded in latest Cretaceous to middle Eocene garnet growth during crustal thickening in the Grouse Creek Mountains, was synchronous with shortening in the foreland fold and thrust belt, including movement on the Absaroka (Late), Medicine Butte, and Hogsback thrusts [*Yonkee et al.*, 1997; *DeCelles*, 2004], as well as shortening in the Laramide foreland province [*Dickinson et al.*, 1988] (Figures 1 and 2). Late Cretaceous extension at the latitude of northernmost Utah, while synchronous with early shortening in the Laramide foreland province (Figure 9c), predated, and thus could thus not have driven, Paleocene to Eocene shortening in the Laramide province (Figure 9d) [cf. *Livaccari*, 1991].

4.3. Eocene Shortening to Extension Transition

[46] The transition from shortening to extension that marked the end of the Laramide orogeny is perhaps the best understood, from a geodynamic standpoint, of the Late Cretaceous to Eocene tectonic mode switches in the western U.S.. In the Idaho-Utah-Wyoming salient of the fold-thrust belt, shortening ended by 54–51 Ma and extensional collapse of the thrust belt began by 49 Ma [*Constenius*, 1996]. Shortening in the Laramide foreland province north of 42°N ended by the middle Eocene (55–50 Ma), but continued south of 42°N until the Late Eocene (40–35 Ma) [*Dickinson et al.*, 1988; *DeCelles*, 2004]. On a regional scale, it has been well demonstrated that the leading edge of a belt of magmatism swept to the southwest from late Paleocene (51°N) to early Late Eocene (39°N) [*Armstrong and Ward*, 1991; *Axen et al.*, 1993; *Constenius*, 1996]. The initiation of extension roughly tracked this migration in magmatism [*Wernicke*, 1992; *Dickinson*, 2002]. The southward sweep

in initiation of magmatism has been viewed as a migratory volcanic arc [*Dickinson*, 2002] related to progressive slab rollback into a down-buckled foundering keel of Farallon slab in the central Basin and Range at the latitude of Las Vegas, Nevada [*Humphreys*, 1995]. Regardless of the mechanism and geometry of removal of the Farallon slab from beneath the Sevier-Laramide hinterland, upwelling of asthenosphere to the base of continental North American lithosphere was associated with a period of decreasing convergence rate between the Farallon and North American plates [*Engebretson et al.*, 1985; *Stock and Molnar*, 1988]. Eocene extension was driven by the combination of gravitational potential energy resulting from thickened Sevier-Laramide crust, removal of the Farallon slab, and upwelling asthenosphere, as well as a decrease in compressional forces transmitted across the plate boundary through decreased plate coupling [*Humphreys*, 1995; *Sonder and Jones*, 1999; *Dickinson*, 2002; *Rahl et al.*, 2002].

5. Conclusions

[47] We have presented evidence for two cycles of shortening followed by extensional exhumation during continuous plate convergence, from the Late Cretaceous to early Tertiary Sevier-Laramide orogen. Complex kinematic histories, such as those presented here, challenge the simple two-stage conceptual model of an orogenic cycle of crustal thickening dominated by inter-plate compressional forces followed by orogenic collapse dominated by intraplate gravitational forces. This adds to the growing body of evidence for alternations in shortening and extension during mountain building [*Platt*, 1986; *Froitzheim et al.*, 1994; *Balanyá et al.*, 1997; *Rawling and Lister*, 1999; *Lister et al.*, 2001; *Collins*, 2002; *Beltrando et al.*, 2007], suggesting that the balance between intraplate gravitational forces and interplate compressional forces may fluctuate cyclically during plate convergence. The cycle from the Sevier hinterland may record orogenic wedge mechanics related to underplating and internal thickening on western thrusts [e.g., *Platt*, 1986; *Goldstein et al.*, 2005; *Cello and Mazzoli*, 1996; *Crespi et al.*, 1996], however, we interpret the heating during decompression to support exhumation as a response to delamination of mantle lithosphere. Subsidence, reinforced by convergent flow, during development and downwelling of a RT instability, may explain the ~86 Ma shortening event in the interior of the orogenic wedge and the development of metamorphic field gradients common in the metamorphic core complexes of the Sevier-Laramide hinterland. Major events of shortening and synconvergent extension internal to the wedge — such as the ~7.5 km of burial and ~10 km of exhumation documented here — in the absence of accretionary events followed by slab rollback [e.g., *Collins*, 2002] may require delamination as a geodynamic driver.

[48] Episodic delamination during continuous subduction provides an alternative mechanism to episodic slab rollback in explaining cyclic tectonic mode switches. Episodicity of this process is consistent with numerical simulations of the delamination process that suggest lithospheric mantle needs to be sufficiently softened by heat and/or by strain to lower the viscosity such that it can flow and participate in the developing mantle drip [*Conrad and Molnar*, 1999]. The availability of high density and low viscosity mantle sufficiently weak to flow leads to the concept of "available buoyancy" wherein mantle lithosphere may be thinned through successive cycles, each stripping the "available buoyancy" from the thickened mantle lithosphere [*Conrad and Molnar*, 1999]. Additionally, the delamination cycle is promoted by active plate convergence. Not only is shortening important in initially developing the instability, but active shortening accelerates growth of the instability [*Molnar et al.*, 1998; *Conrad*, 2000]. Thus, synconvergent delamination is more probable than post-convergent delamination, and it can probably occur episodically during protracted plate convergence and mountain building.

Appendix A

[49] Whole rocks were crushed using a porcelain mortar and pestle at Northern Arizona University to disaggregate the garnet fragments from the matrix and to crush the garnet into smaller fragments. The resulting garnet fragments were handpicked under a binocular microscope to obtain fragments as free as possible of visible inclusions such as ilmenite and biotite. Six 200–250 mg fractions of visually clear garnet and ~250 mg of bulk rock were selected for isotopic analysis. Garnet and whole rock separates were finely crushed at Washington State University using a diamonite® mortar and pestle to ~30 μm size prior to dissolution. Whole rock powders were digested in high-pressure Teflon bombs, and garnet separates were digested via hotplate dissolution in Savillex beakers. Samples were spiked with a mixed ^{176}Lu-^{180}Hf tracer to determine the concentrations of Lu and Hf and accurately determine ^{176}Lu/^{177}Hf ratios for geochronology. Chromatographic separation of Lu and Hf was performed using ion-exchange columns as outlined by *Cheng et al.* [2008]. The isotopic compositions of Lu and Hf were analyzed using the ThermoFinnigan Neptune MC-ICP-MS at Washington State University. Given the low concentration of Hf in samples from this study (typically <1 ppm), Hf samples were introduced as dry aerosols using an Aridus microconcentric desolvating nebulizer (Cetac Inc.) in order to provide more sensitivity for Hf analysis on the Neptune. The Hf sample solutions were concentration matched to external standard JMC 475 prior to analysis, and measured relative to this standard. Each individual analytical session was normalized to the accepted ^{176}Hf/^{177}Hf value of 0.282160 for JMC 475 [*Vervoort and Blichert-Toft*, 1999]. Data corrections for isobaric interferences and mass fractionation of Lu and Hf isotopes were performed as reported by *Vervoort et al.* [2004].

[50] **Acknowledgments.** This research was funded by National Science Foundation grants EAR-061009 to M.L.W., EAR-0061048 to T.D.H., and EAR-0609856 to J.D.V. Clint Conrad is thanked for discussions on Rayleigh-Taylor instabilities. Constructive comments by Editor T. Ehlers, Associate Editor M. Rushmore, journal reviewer R. Miller, and an anonymous reviewer are appreciated.

References

Allmendinger, R. W. (1992), Fold and thrust tectonics of the Western United States exclusive of the accreted terranes, in *The Cordilleran Orogen: Conterminous U.S.*, *Geol. North Am.*, vol. G-3, edited by B. C. Burchfiel, P. W. Lipman, and M. L. Zoback, pp. 583–607, Geol. Soc. of Am, Boulder, Colo.

Anczkiewicz, R., J. Szczepański, S. Mazur, C. Storey, Q. Crowley, and I. M. Villa (2007), Lu–Hf geochronology and trace element distribution

in garnet: Implications for uplift and exhumation of ultra-high pressure granulites in the Sudetes, SW Poland, *Lithos*, *95*, 363–380, doi:10.1016/j.lithos.2006.09.001.

Annen, C., and R. S. J. Sparks (2002), Effects of repetitive emplacement of basaltic intrusions on thermal evolution and melt generation in the crust, *Earth Planet. Sci. Lett.*, *203*, 937–955, doi:10.1016/S0012-821X(02)00929-9.

Armstrong, R. L. (1968), Sevier orogenic belt in Nevada and Utah, *Geol. Soc. Am. Bull.*, *79*, 429–458, doi:10.1130/0016-7606(1968)79[429:SOBINA]2.0.CO;2.

Armstrong, R. L. (1982), Cordilleran metamorphic core complexes-From Arizona to southern Canada, *Annu. Rev. Earth Planet. Sci.*, *10*, 129–154, doi:10.1146/annurev.ea.10.050182.001021.

Armstrong, R. L., and P. Ward (1991), Evolving geographic patterns of Cenozoic magmatism in the North American Cordillera: The temporal and spatial association of magmatism and metamorphic core complexes, *J. Geophys. Res.*, *96*, 13,201–13,224, doi:10.1029/91JB00412.

Atwater, T., and J. M. Stock (1998), Pacific-North America plate tectonics of the Neogene southwestern United States: An update, *Int. Geol. Rev.*, *40*, 375–402, doi:10.1080/00206819809465216.

Axen, G. J., W. J. Taylor, and J. M. Bartley (1993), Space-time patterns and tectonic controls of Tertiary extension and magmatism in the Great Basin of the western United States, *Geol. Soc. Am. Bull.*, *105*, 56–76, doi:10.1130/0016-7606(1993)105<0056:STPATC>2.3.CO;2.

Balanyá, J. C., V. García-Dueñas, and J. M. Azañón (1997), Alternating contractional and extensional events in the Alpujarride nappes of the Alboran Domain (Betics, Gibraltar Arc), *Tectonics*, *16*, 226–238, doi:10.1029/96TC03871.

Barth, A. P., and J. S. Schneiderman (1996), A comparison of structures in the Andean Orogen of northern Chile and exhumed midcrustal structures in southern California, USA: An analogy in tectonic style?, *Int. Geol. Rev.*, *38*, 1075–1085, doi:10.1080/00206819709465383.

Barton, M. D. (1990), Cretaceous magmatism, metamorphism, and metallogeny in the east-central Great Basin, in *The Nature and Origin of Cordilleran Magmatism*, edited by J. L. Anderson, *Mem. Geol. Soc. Am.*,*174*, 283–302.

Beltrando, M., J. Hermann, G. Lister, and R. Compagnoni (2007), On the evolution of orogens: Pressure cycles and deformation mode switches, *Earth Planet. Sci. Lett.*, *256*, 372–388, doi:10.1016/j.epsl.2007.01.022.

Beltrando, M., G. Lister, J. Hermann, M. Forster, and R. Compagnoni (2008), Deformation mode switches in the Penninic units of the Urtier Valley (Western Alps): Evidence for a dynamic orogen, *J. Struct. Geol.*, *30*, 194–219, doi:10.1016/j.jsg.2007.10.008.

Bird, P. (1984), Laramide crustal thickening event in the Rocky Mountain foreland and Great Plains, *Tectonics*, *3*, 741–758, doi:10.1029/TC003i007p00741.

Bouvier, A., J. D. Vervoort, and P. J. Patchett (2008), The Lu-Hf and Sm-Nd isotopic composition of CHUR: Constraints from unequilibrated chondrites and implications for the bulk composition of terrestrial planets, *Earth Planet. Sci. Lett.*, *273*, 48–57, doi:10.1016/j.epsl.2008.06.010.

Braun, I., J.-M. Montel, and C. Nicollet (1998), Electron microprobe dating of monazites from high-grade gneisses and pegmatites of the Kerala Khondalite Belt, southern India, *Chem. Geol.*, *146*, 65–85, doi:10.1016/S0009-2541(98)00005-9.

Burchfiel, B. C., and L. H. Royden (1985), North-south extension within the convergent Himalayan region, *Geology*, *13*, 679–682, doi:10.1130/0091-7613(1985)13<679:NEWTCH>2.0.CO;2.

Camilleri, P. A. (1998), Prograde metamorphism, strain evolution, and collapse of footwalls of thick thrust sheets, a case study from the Mesozoic Sevier hinterland, U.S.A, *J. Struct. Geol.*, *20*, 1023–1042, doi:10.1016/S0191-8141(98)00032-7.

Camilleri, P. A., and K. R. Chamberlain (1997), Mesozoic tectonics and metamorphism in the Pequop Mountains and Wood Hills region, northeast Nevada: Implications for the architecture and evolution of the Sevier orogen, *Geol. Soc. Am. Bull.*, *109*, 74–94, doi:10.1130/0016-7606(1997)109<0074:MTAMIT>2.3.CO;2.

Camilleri, P. A., W. A. Yonkee, J. C. Coogan, P. G. DeCelles, A. McGrew, and M. Wells (1997), Hinterland to foreland transect through the Sevier orogen, NE Nevada to SW Wyoming: Structural style, metamorphism, and kinematic history of a large contractional orogenic wedge, in *Proterozoic to Recent Stratigraphy, Tectonics, and Volcanology, Utah, Nevada, Southern Idaho and Central Mexico*, edited by P. K. Link and B. J. Kowallis, *Brigham Young Univ. Geol. Stud.*, *42*, part 1, 297–309.

Carrapa, B., L. Schoenbohm, P. DeCelles, M. T. Clementz, and K. Huntington (2009), Surface response to lithospheric delamniation: An example from the Puna plateau of NW Argentina, *Geol. Soc. Am. Abstr. Programs*, *41*, 516.

Cello, G., and S. Mazzoli (1996), Extensional processes driven by large-scale duplexing in collisional regimes, *J. Struct. Geol.*, *18*, 1275–1279, doi:10.1016/S0191-8141(96)00054-5.

Cheng, H., R. L. King, E. Nakamura, J. D. Vervoort, and Z. Zhou (2008), Coupled Lu-Hf and Sm-Nd geochronology constrains garnet growth in ultra-high-pressure eclogites from the Dabie orogen, *J. Metamorph. Geol.*, *26*, 741–758, doi:10.1111/j.1525-1314.2008.00785.x.

Cherniak, D. J., E. B. Watson, M. Grove, and T. M. Harrison (2004), Pb diffusion in monazite: A combined RBS/SIMS study, *Geochim. Cosmochim. Acta*, *68*, 829–840, doi:10.1016/j.gca.2003.07.012.

Cobbold, P. R., and H. Quinquis (1980), Development of sheath folds in shear regimes, *J. Struct. Geol.*, *5*, 383–399.

Collins, W. J. (2002), Hot orogens, tectonic switching, and creation of continental crust, *Geology*, *30*, 535–538, doi:10.1130/0091-7613(2002)030<0535:HOTSAC>2.0.CO;2.

Compton, R. R., V. R. Todd, R. E. Zartman, and C. W. Naeser (1977), Oligocene and Miocene metamorphism, folding, and low-angle faulting in northwestern Utah, *Geol. Soc. Am. Bull.*, *88*, 1237–1250, doi:10.1130/0016-7606(1977)88<1237:OAMMFA>2.0.CO;2.

Coney, P. J., and T. A. Harms (1984), Cordilleran metamorphic core complexes: Cenozoic extensional relics of Mesozoic compression, *Geology*, *12*, 550–554, doi:10.1130/0091-7613(1984)12<550:CMCCCE>2.0.CO;2.

Coney, P. J., and S. J. Reynolds (1977), Cordilleran Benioff zones, *Nature*, *270*, 403–406, doi:10.1038/270403a0.

Conrad, C. P. (2000), Convective instability of thickening mantle lithosphere, *Geophys. J. Int.*, *143*, 52–70, doi:10.1046/j.1365-246x.2000.00214.x.

Conrad, C. P., and P. Molnar (1999), Convective instability of a boundary layer with temperature- and strain-rate-dependent viscosity in terms of "available buoyancy," *Geophys. J. Int.*, *139*, 51–68, doi:10.1046/j.1365-246X.1999.00896.x.

Constenius, K. N. (1996), Late Paleogene extensional collapse of the Cordilleran foreland fold and thrust belt, *Geol. Soc. Am. Bull.*, *108*, 20–39, doi:10.1130/0016-7606(1996)108<0020:LPECOT>2.3.CO;2.

Cooper, F. J., J. P. Platt, R. Anczkiewicz, and M. J. Whitehouse (2010), Footwall dip of a core complex detachment fault: Thermobarometric constraints from the northern Snake Range (Basin and Range, USA), *J. Metamorph. Geol.*, *28*, 997–1020, doi:10.1111/j.1525-1314.2010.00907.x.

Crespi, J. M., Y.-C. Chan, and M. S. Swaim (1996), Synorogenic extension and exhumation of the Taiwan hinterland, *Geology*, *24*, 247–250, doi:10.1130/0091-7613(1996)024<0247:SEAEOT>2.3.CO;2.

Cruz-Uribe, A. M. (2008) Pressure-temperature-time paths constraining the ages of thrusting in the Sevier hinterland, MS thesis, 112 pp., North. Ariz. Univ., Flagstaff.

Cruz-Uribe, A. M., T. D. Hoisch, M. L. Wells, and J. D. Vervoort (2008), Ages of Sevier thrusting from dating of metamorphic garnet using the Lu-Hf method, *Eos Trans. AGU*, *89*(53), Fall Meet. Suppl., Abstract T23C-2062.

Dahlen, F. A. (1984), Noncohesive critical Coulomb wedges: An exact solution, *J. Geophys. Res.*, *89*, 10,125–10,133, doi:10.1029/JB089iB12p10125.

Dalmayrac, B., and P. Molnar (1981), Parallel thrust and normal faulting in Peru and the constraints on the state of stress, *Earth Planet. Sci. Lett.*, *55*, 473–481, doi:10.1016/0012-821X(81)90174-6.

Davis, D., J. Suppe, and F. A. Dahlen (1983), Mechanics of fold-and-thrust belts and accretionary wedges, *J. Geophys. Res.*, *88*, 1153–1172, doi:10.1029/JB088iB02p01153.

de Capitani, C., and K. Petrakakis (2010), The computation of equilibrium assemblage diagrams with Theriak/Domino software, *Am. Mineral.*, *95*, 1006–1016, doi:10.2138/am.2010.3354.

DeCelles, P. G. (1994), Late Cretaceous-Paleocene synorogenic sedimentation and kinematic history of the Sevier thrust belt, northeast Utah and southwest Wyoming, *Geol. Soc. Am. Bull.*, *106*, 32–56, doi:10.1130/0016-7606(1994)106<0032:LCPSSA>2.3.CO;2.

DeCelles, P. G. (2004), Late Jurassic to Eocene evolution of the Cordilleran thrust belt and foreland basin system, western U.S.A, *Am. J. Sci.*, *304*, 105–168, doi:10.2475/ajs.304.2.105.

DeCelles, P. G., and J. C. Coogan (2006), Regional structure and kinematic history of the Sevier fold-and-thrust belt, central Utah, *Geol. Soc. Am. Bull.*, *118*, 841–864, doi:10.1130/B25759.1.

DeCelles, P. G., and B. S. Currie (1996), Long-term sediment accumulation in the Middle Jurassic-early Eocene Cordilleran retroarc foreland basin system, *Geology*, *24*, 591–594, doi:10.1130/0091-7613(1996)024<0591:LTSAIT>2.3.CO;2.

DeCelles, P. G., and G. Mitra (1995), History of the Sevier orogenic wedge in terms of critical taper models, northeast Utah and southwest Wyoming, *Geol. Soc. Am. Bull.*, *107*, 454–462, doi:10.1130/0016-7606(1995)107<0454:HOTSOW>2.3.CO;2.

DeCelles, P. G., T. F. Lawton, and G. Mitra (1995), Thrust timing, growth of structural culminations, and synorogenic sedimentation in the type Sevier orogenic belt, western United States, *Geology*, *23*, 699–702, doi:10.1130/0091-7613(1995)023<0699:TTGOSC>2.3.CO;2.

DeCelles, P. G., M. N. Ducea, P. Kapp, and G. Zandt (2009), Cyclicity in Cordilleran orogenic systems, *Nat. Geosci.*, *2*, 251–257, doi:10.1038/ngeo469.

Dewey, J. F. (1988), Extensional collapse of orogens, *Tectonics*, *7*, 1123–1139, doi:10.1029/TC007i006p01123.

DeWolf, C. P., N. Belshaw, and R. K. O'Nions (1993), A metamorphic history from micron-scale $^{207}Pb/^{206}Pb$ chronometry of Archaean monazite, *Earth Planet. Sci. Lett.*, *120*, 207–220, doi:10.1016/0012-821X(93)90240-A.

Dickinson, W. R. (2002), The Basin and Range province as a composite extensional domain, *Int. Geol. Rev.*, *44*, 1–38, doi:10.2747/0020-6814.44.1.1.

Dickinson, W. R., M. A. Klute, J. Michael, S. U. Janecke, E. R. Lundin, M. A. McKittrick, and M. D. Olivares (1988), Paleogeographic and paleotectonic setting of Laramide sedimentary basins in the central Rock Mountains region, *Geol. Soc. Am. Bull.*, *100*, 1023–1039, doi:10.1130/0016-7606(1988)100<1023:PAPSOL>2.3.CO;2.

Ducea, M. (2001), The California arc: Thick granitic batholiths, eclogitic residues, lithospheric-scale thrusting, and magmatic flare-ups, *GSA Today*, *11*, 4–10, doi:10.1130/1052-5173(2001)011<0004:TCATGB>2.0.CO;2.

Ducea, M. (2002), Constraints on the bulk composition and root foundering rates of continental arcs: A California arc perspective, *J. Geophys. Res.*, *107*(B11), 2304, doi:10.1029/2001JB000643.

Engebretson, D. C., A. Cox, and R. G. Gordon (1985), *Relative Motions Between Oceanic and Continental Plates in the Pacific Basin*, *Spec. Pap. Geol. Soc. Am.*, *206*, 59 pp.

England, P. C., and G. Houseman (1989), Extension during continental convergence, with application to the Tibetan Plateau, *J. Geophys. Res.*, *94*, 17,561–17,579, doi:10.1029/JB094iB12p17561.

England, P. E., and A. B. Thompson (1984), Pressure-temperature-time paths of regional metamorphism, I, Heat transfer during the evolution of regions of thickened crust, *J. Petrol.*, *97*, 894–928.

Erslev, E. A. (1993), Thrusts, back-thrusts and detachment of Rocky Mountain foreland arches, in *Laramide Basement Deformation in the Rocky Mountain Foreland of the Western United States*, edited by C. J. Schmidt, R. B. Chase, E. A. and Erslev, *Spec. Pap. Geol. Soc. Am.*, *280*, 339–358.

Foster, G., P. Kinny, D. Vance, C. Prince, and N. Harris (2000), The significance of monazite U–Th–Pb age data in metamorphic assemblages: A combined study of monazite and garnet chronometry, *Earth Planet. Sci. Lett.*, *181*, 327–340, doi:10.1016/S0012-821X(00)00212-0.

Froitzheim, N. (1992), Formation of recumbent folds during synorogenic crustal extension (Austroalpine nappes, Switzerland), *Geology*, *20*, 923–926, doi:10.1130/0091-7613(1992)020<0923:FORFDS>2.3.CO;2.

Froitzheim, N., S. M. Schmid, and P. Conti (1994), Repeated change from crustal shortening to orogen-parallel extension in the Austroalpine units of Graubunden, *Eclogae Geol. Helv.*, *87*, 559–612.

Goldstein, A., B. Selleck, and J. W. Valley (2005), Pressure, temperature, and composition history of syntectonic fluids in a low-grade metamorphic terrane, *Geology*, *33*, 421–424, doi:10.1130/G21143.1.

Grove, M., C. E. Jacobson, A. P. Barth, and A. Vucic (2003), Temporal and spatial trends of Late Cretaceous-early Tertiary underplating of Pelona and related schist beneath southern California and southwestern Arizona, in *Tectonic Evolution of Northwestern Mexico and Southwestern USA*, edited by S. E. Johnson et al., *Spec. Pap. Geol. Soc. Am.*, *374*, 381–406.

Handy, M. R., A. Mulch, M. Rosenau, and C. L. Rosenberg (2001), The role of fault zones and melts as agents of weakening, hardening and differentiation of the continental crust; as synthesis, in *The Nature and Tectonic Significance of Fault Zone Weakening*, edited by R. Holdsworth et al., *Geol. Soc. Spec. Publ.*, *186*, 305–332.

Harris, C. R., T. D. Hoisch, and M. L. Wells (2007), Construction of a composite pressure-temperature path: Revealing the synorogenic burial and exhumation history of the Sevier hinterland, USA, *J. Metamorph. Geol.*, *25*, 915–934, doi:10.1111/j.1525-1314.2007.00733.x.

Heller, P. L., S. S. Bowler, H. P. Chambers, J. C. Coogan, E. S. Hagen, M. W. Shuster, N. S. Winslow, and T. F. Lawton (1986), Time of initial thrusting in the Sevier orogenic belt, Idaho, Wyoming and Utah, *Geology*, *14*, 388–391, doi:10.1130/0091-7613(1986)14<388:TOITIT>2.0.CO;2.

Henderson, L. J., R. G. Gordon, and D. C. Engebretsen (1984), Mesozoic aseismic ridges on the Farallon plate and southward migration of shallow subduction during the Laramide orogeny, *Tectonics*, *3*, 121–132, doi:10.1029/TC003i002p00121.

Hodges, K. V., and J. D. Walker (1992), Extension in the Cretaceous Sevier orogen, North American Cordillera, *Geol. Soc. Am. Bull.*, *104*, 560–569, doi:10.1130/0016-7606(1992)104<0560:EITCSO>2.3.CO;2.

Hoisch, T. D., and C. Simpson (1993), Rise and tilt of metamorphic rocks in the lower plate of a detachment fault in the Funeral Mountains, Death Valley, California, *J. Geophys. Res.*, *98*, 6805–6827, doi:10.1029/92JB02411.

Hoisch, T. D., M. L. Wells, and L. M. Hanson (2002), Pressure-temperature paths from garnet zoning: Evidence for multiple episodes of thrust burial in the hinterland of the Sevier orogenic belt, *Am. Mineral.*, *87*, 115–131.

Hoisch, T. D., M. L. Wells, and M. Grove (2008), Age trends in garnet-hosted monazite inclusions from upper amphibolite facies schist in the northern Grouse Creek Mountains, Utah, *Geochim. Cosmochim. Acta*, *72*, 5505–5520, doi:10.1016/j.gca.2008.08.012.

Holdaway, M. J. (2000), Application of new experimental and garnet Margules data to the garnet-biotite geothermometer, *Am. Mineral.*, *85*, 881–892.

Holland, T. J. B., and R. Powell (1998), An internally consistent thermodynamic data set for phases of petrological interest, *J. Metamorph. Geol.*, *16*, 309–343, doi:10.1111/j.1525-1314.1998.00140.x.

Houseman, G. A., and P. Molnar (1997), Gravitational (Rayleigh-Taylor) instability of a layer with non-linear viscosity and convective thinning of continental lithosphere, *Geophys. J. Int.*, *128*, 125–150, doi:10.1111/j.1365-246X.1997.tb04075.x.

Houseman, G. A., D. P. McKenzie, and P. Molnar (1981), Convective instability of a thickened boundary layer and its relevance for the thermal evolution of continental convergent belts, *J. Geophys. Res.*, *86*, 6115–6132, doi:10.1029/JB086iB07p06115.

Howard, K. A. (2003), Crustal structure in the Elko-Carlin region, Nevada, during Eocene gold mineralization: Ruby-East Humboldt metamorphic core complex as a guide to the deep crust, *Econ. Geol.*, *98*, 249–268, doi:10.2113/98.2.249.

Hudec, M. R. (1992), Mesozoic structural and metamorphic history of the central Ruby Mountains metamorphic core complex, Nevada, *Geol. Soc. Am. Bull.*, *104*, 1086–1100, doi:10.1130/0016-7606(1992)104<1086:MSAMHO>2.3.CO;2.

Humphreys, E. D. (1995), Post-Laramide removal of the Farallon slab, western United States, *Geology*, *23*, 987–990, doi:10.1130/0091-7613(1995)023<0987:PLROTF>2.3.CO;2.

Jamieson, R. A., C. Beaumont, P. Fullsack, and B. Lee (1998), Barrovian regional metamorphism: Where's the heat?, in *What Drives Metamorphism and Metamorphic Reactions?*, edited by P. J. Treloar and P. J. O'Brien, *Geol. Soc. Spec. Publ.*, *138*, 23–51.

Jolivet, L., and J.-P. Brun (2010), Cenozoic geodynamic evolution of the Aegean, *Int. J. Earth Sci.*, *99*, 109–138, doi:10.1007/s00531-008-0366-4.

Jordan, T., B. Isacks, R. Allmendinger, J. Brewer, V. Ramos, and C. Ando (1983), Andean tectonics related to the geometry of the subducted plate, *Geol. Soc. Am. Bull.*, *94*, 341–361, doi:10.1130/0016-7606(1983)94<341:ATRTGO>2.0.CO;2.

Kohlstedt, D. L., B. Evans, and S. J. Mackwell (1995), Strength of the lithosphere: Constraints imposed by laboratory experiments, *J. Geophys. Res.*, *100*, 17,587–17,602, doi:10.1029/95JB01460.

Kohn, M. J. (1993), Uncertainties in differential thermodynamic (Gibbs' method) P-T paths, *Contrib. Mineral. Petrol.*, *113*, 24–39, doi:10.1007/BF00320829.

Kohn, M. J., and F. S. Spear (1991), Error propagation for barometers 2: Application to natural rocks, *Am. Mineral.*, *76*, 138–147.

Labotka, T. C. (1980), Petrology of a medium-pressure regional metamorphism terrain, Funeral Mountains, California, *Am. Mineral.*, *65*, 670–689.

Lewis, C., B. P. Wernicke, J. Selverstone, and J. M. Bartley (1999), Deep burial of the footwall of the northern Snake Range decollement, Nevada, *Geol. Soc. Am. Bull.*, *111*, 39–51, doi:10.1130/0016-7606(1999)111<0039:DBOTFO>2.3.CO;2.

Lister, G. S., M. A. Forster, and T. J. Rawling (2001), Episodicity during orogenesis, in *Continental Reactivation and Reworking*, edited by J. A. Miller et al., *Geol. Soc. Spec. Publ.*, *184*, 89–113, doi:10.1144/GSL.SP.2001.184.01.06.

Liu, L., S. Spasojevic, and M. Gurnis (2008), Reconstructing Farallon plate subduction beneath North American back to the Late Cretaceous, *Science*, *322*, 934–938, doi:10.1126/science.1162921.

Liu, L., M. Gurnis, M. Seton, J. Saleeby, R. D. Müller, and J. M. Jackson (2010), The role of oceanic plateau subduction in the Laramide orogeny, *Nat. Geosci.*, *3*, 353–357, doi:10.1038/ngeo829.

Liu, S., and D. Nummedal (2004), Late Cretaceous subsidence in Wyoming: Quantifying the dynamic component, *Geology*, *32*, 397–400, doi:10.1130/G20318.1.

Livaccari, R. F. (1991), Role of crustal thickening and extensional collapse in the tectonic evolution of the Sevier-Laramide Orogeny, Western United States, *Geology*, *19*, 1104–1107, doi:10.1130/0091-7613(1991)019<1104:ROCTAE>2.3.CO;2.

Livaccari, R. F., and F. V. Perry (1993), Isotopic evidence for preservation of Cordilleran lithospheric mantle during the Sevier-Laramide Orogeny, Western United States, *Geology*, *21*, 719–722, doi:10.1130/0091-7613(1993)021<0719:IEFPOC>2.3.CO;2.

Malavieille, J. (1987), Kinematics of compressional and extensional ductile shearing deformation in a metamorphic core complex of the northeastern

Basin and Range, *J. Struct. Geol.*, *9*, 541–554, doi:10.1016/0191-8141(87)90139-8.

Mattinson, C. G., J. P. Colgan, J. R. Metcalf, and E. L. Miller (2007), Late Cretaceous to Paleocene metamorphism and magmatism in the Funeral Mountains metamorphic core complex, Death Valley, California, *Spec. Pap. Geol. Soc. Am.*, *419*, 205–224.

McGrew, A. J., M. T. Peters, and J. E. Wright (2000), Thermobarometric constraints on the tectonothermal evolution of the East Humboldt Range metamorphic core complex, Nevada, *Geol. Soc. Am. Bull.*, *112*, 45–60, doi:10.1130/0016-7606(2000)112<45:TCOTTE>2.0.CO;2.

McKenzie, D. (1978), Some remarks on the development of sedimentary basins, *Earth Planet. Sci. Lett.*, *40*, 25–32, doi:10.1016/0012-821X(78)90071-7.

Miller, C. F., and L. J. Bradfish (1980), An inner Cordilleran belt of muscovite-bearing plutons, *Geology*, *8*, 412–416, doi:10.1130/0091-7613(1980)8<412:AICBOM>2.0.CO;2.

Miller, D. M. (1980), Structural geology of the northern Albion Mountains, south-central Idaho, in *Cordilleran Metamorphic Core Complexes*, edited by M. D. Crittenden, P. J. Coney, and G. H. Davis, *Mem. Geol. Soc. Am.*, *153*, 399–423.

Miller, D. M. (1983), Allochthonous quartzite sequence in the Albion Mountains, Idaho, and proposed Proterozoic Z and Cambrian correlatives in the Pilot Range, Utah and Nevada, in *Tectonic and Stratigraphic Studies in the Eastern Great Basin*, edited by D. M. Miller, V. R. Todd, and K. A. Howard, *Mem. Geol. Soc. Am.*, *157*, 191–213.

Miller, D. M., and T. D. Hoisch (1995), Jurassic tectonics of northeastern Nevada and northwestern Utah from the perspective of barometric studies, in *Jurassic Magmatism and Tectonics of the North American Cordillera*, edited by D. M. Miller and C. Busby, *Spec. Pap. Geol. Soc. Am.*, *299*, 267–294.

Miller, D. M., J. E. Repetski, and A. G. Harris (1991), East-trending Paleozoic continental margin near Wendover, Utah, in *Paleozoic Paleogeography of the Western United States*, edited by J. D. Cooper and C. H. Stevens, *Spec. Publ. Pac. Sect. SEPM*, *67*, 439–461.

Miller, E. L., P. B. Gans, J. E. Wright, and J. F. Sutter (1988), Metamorphic history of east-central Basin and Range Province, in *Metamorphism and Crustal Evolution of the Western United States*, *Rubey Vol.*, vol. 7, edited by W. G. Ernst, pp. 649–682, Prentice Hall, Englewood Cliffs, N. J.

Molnar, P., and H. Lyon-Caen (1988), Some simple physical aspects of the support, structure and evolution of mountain belts, in *Processes in Continental and Lithospheric Deformation*, edited by S. P.-J. Clark, *Spec. Pap. Geol. Soc. Am.*, *218*, 179–207.

Molnar, P., G. A. Houseman, and C. P. Conrad (1998), Rayleigh-Taylor instability and convective thinning of mechanically thickened lithosphere: Effects of non-linear viscosity decreasing exponentially with depth and of horizontal shortening of the layer, *Geophys. J. Int.*, *133*, 568–584, doi:10.1046/j.1365-246X.1998.00510.x.

Montel, J.-M., S. Foret, and D. Vielzeuf (2000), Preservation of old U–Th–Pb ages in shielded monazite: Example from Beni Bousera Hercynian kinzigites (Morocco), *J. Metamorph. Geol.*, *18*, 335–342, doi:10.1046/j.1525-1314.2000.00261.x.

Müller, R. D., W. R. Roest, J.-Y. Royer, L. M. Gahagan, and J. G. Sclater (1997), Digital isochrons of the world's ocean floor, *J. Geophys. Res.*, *102*, 3211–3214, doi:10.1029/96JB01781.

Patiño Douce, A. E. (1999), What do experiments tell us about the relative contributions of crust and mantle to the origin of granitic magmas?, in *Understanding Granites: Integrating New and Classical Techniques*, edited by A. Castro et al., *Geol. Soc. Spec. Publ.*, *168*, 55–75.

Platt, J. P. (1986), Dynamics of orogenic wedges and the uplift of high-pressure metamorphic rocks, *Geol. Soc. Am. Bull.*, *97*, 1037–1053, doi:10.1130/0016-7606(1986)97<1037:DOOWAT>2.0.CO;2.

Platt, J. P., and P. C. England (1994), Convective removal of lithosphere beneath mountain belts: Thermal and mechanical consequences, *Am. J. Sci.*, *294*, 307–336, doi:10.2475/ajs.294.3.307.

Poitrasson, F., S. Cheney, and D. J. Bland (1996), Contrasted monazite hydrothermal alteration mechanisms and their geochemical implications, *Earth Planet. Sci. Lett.*, *145*, 79–96, doi:10.1016/S0012-821X(96)00193-8.

Rahl, J. M., A. J. McGrew, and K. A. Foland (2002), Transition from contraction to extension in the northeastern Basin and Range: New evidence from the Copper Mountains, Nevada, *J. Geol.*, *110*, 179–194, doi:10.1086/338413.

Rawling, T. J., and G. Lister (1999), Oscillating modes of orogeny in the Southwest Pacific and the tectonic evolution of New Caledonia, in *Exhumation Processes: Normal Faulting, Ductile Flow and Erosion*, edited by U. Ring et al., *Geol. Soc. Spec. Publ.*, *154*, 109–127.

Rey, P., O. Vanderhaeghe, and C. Teyssier (2001), Gravitational collapse of the continental crust: Definition, regimes and modes, *Tectonophysics*, *342*, 435–449, doi:10.1016/S0040-1951(01)00174-3.

Rossetti, F., C. Faccenna, and G. Ranalli (2002), The influence of backstop dip and convergence velocity in the growth of viscous doubly vergent orogenic wedges: Insights from thermomechanical laboratory experiments, *J. Struct. Geol.*, *24*, 953–962, doi:10.1016/S0191-8141(01)00127-4.

Royden, L. H. (1993), Evolution of retreating subduction boundaries formed during continental collision, *Tectonics*, *12*, 629–638, doi:10.1029/92TC02641.

Royse, F., Jr., M. A. Warner, and D. L. Reese (1975), Thrust belt structural geometry and related stratigraphic problems Wyoming Idaho-northern Utah, in *Deep Drilling Frontiers of the Central Rocky Mountains*, edited by D. W. Bolyard, pp. 41–54, Rocky Mt. Assoc. of Geol., Denver, Colo.

Saleeby, J. (2003), Segmentation of the Laramide Slab–Evidence from the southern Sierra Nevada region, *Geol. Soc. Am. Bull.*, *115*, 655–668, doi:10.1130/0016-7606(2003)115<0655:SOTLSF>2.0.CO;2.

Saltzer, S. D., and K. V. Hodges (1988), The Middle Mountain shear zone, southern Idaho: Kinematic analysis of an early Tertiary high-temperature detachment, *Geol. Soc. Am. Bull.*, *100*, 96–103, doi:10.1130/0016-7606(1988)100<0096:TMMSZS>2.3.CO;2.

Scherer, E. E., K. L. Cameron, and J. Blichert-Toft (2000), Lu-Hf geochronology: closure temperature relative to the Sm–Nd System and the effects of trace mineral inclusions, *Geochim. Cosmochim. Acta*, *64*, 3413–3432, doi:10.1016/S0016-7037(00)00440-3.

Scherer, E., C. Münker, and K. Mezger (2001), Calibration of the lutetium-hafnium clock, *Science*, *293*, 683–687, doi:10.1126/science.1061372.

Severinghaus, J., and T. Atwater (1990), Cenozoic geometry and thermal state of the subducting slabs beneath western North America, in *Basin and Range Extensional Tectonics Near the Latitude of Las Vegas, Nevada*, edited by B. P. Wernicke, *Mem. Geol. Soc. Am.*, *176*, 1–22.

Simpson, R. L., R. R. Parrish, M. P. Searle, and D. J. Waters (2000), Two episodes of monazite crystallization during metamorphism and crustal melting in the Everest region of the Nepalese Himalaya, *Geology*, *28*, 403–406, doi:10.1130/0091-7613(2000)28<403:TEOMCD>2.0.CO;2.

Söderlund, W., P. J. Patchett, J. D. Vervoort, and C. E. Isachsen (2004), The ^{176}Lu decay constant determined by Lu-Hf and U-Pb isotope systematics of Precambrian mafic intrusions, *Earth Planet. Sci. Lett.*, *219*, 311–324, doi:10.1016/S0012-821X(04)00012-3.

Sonder, L. J., and C. H. Jones (1999), Western United States extension: How the west was widened, *Annu. Rev. Earth Planet. Sci.*, *27*, 417–462, doi:10.1146/annurev.earth.27.1.417.

Spear, F. S., S. M. Peacock, M. J. Kohn, F. P. Florence, and T. Menard (1991), Computer programs for petrologic PT-t path calculations, *Am. Mineral.*, *76*, 2009–2012.

Speed, R. C., M. W. Elison, and R. R. Heck (1988), Phanerozoic tectonic evolution of the Great Basin, in *Metamorphism and Crustal Evolution of the Western United States*, *Rubey Vol.*, vol. 7, edited by W. G. Ernst, pp. 572–605, Prentice Hall, Englewood Cliffs, N. J.

Stern, R. A., and R. G. Berman (2001), Monazite U–Pb and Th–Pb geochronology by ion microprobe, with an application to in situ dating of an Archean metasedimentary rock, *Chem. Geol.*, *172*, 113–130, doi:10.1016/S0009-2541(00)00239-4.

Stock, J. M., and P. Molnar (1988), Uncertainties and implications of the Late Cretaceous and Tertiary position of North America relative to the Farallon, Kula and Pacific plates, *Tectonics*, *7*, 1339–1384, doi:10.1029/TC007i006p01339.

Strickland, A., E. L. Miller, and J. L. Wooden (2011a), The timing of Tertiary metamorphism and deformation in the Albion-Raft River-Grouse Creek metamorphic core complex, Utah and Idaho, *J. Geol.*, *119*, 185–206, doi:10.1086/658294.

Strickland, A., E. L. Miller, J. L. Wooden, R. Kozdon, and J. W. Valley (2011b), Syn-extensional plutonism and peak metamorphism in the Albion-Raft River-Grouse Creek metamorphic core complex, *Am. J. Sci.*, *311*, 261–314, doi:10.2475/04.2011.01.

Taylor, W. J., J. M. Bartley, M. W. Martin, J. W. Geissman, J. D. Walker, P. A. Armstrong, and J. E. Fryxell (2000), Relations between hinterland and foreland shortening: Sevier orogeny, central North American Cordillera, *Tectonics*, *19*, 1124–1143, doi:10.1029/1999TC001141.

Terry, M. P., P. Robinson, M. A. Hamilton, and M. J. Jercinovic (2000), Monazite geochronology of UHP and HP metamorphism, deformation, and exhumation, Nordoyane, Western Gneiss Region, Norway, *Am. Mineral.*, *85*, 1651–1664.

Todd, C. S. (1998), Limits on the precision of geobarometry at low grossular and anorthite content, *Am. Mineral.*, *83*, 1161–1167.

Usui, T., E. Nakamura, K. Kobayashi, S. Maruyama, and H. Helmstaedt (2003), Fate of the subducted Farallon Plate inferred from eclogite xenoliths in the Colorado Plateau, *Geology*, *31*, 589–592, doi:10.1130/0091-7613(2003)031<0589:FOTSFP>2.0.CO;2.

Vanderhaeghe, O., and C. Teyssier (2001), Partial melting and flow of orogens, *Tectonophysics*, *342*, 451–472, doi:10.1016/S0040-1951(01)00175-5.

Vervoort, J. D., and J. Blichert-Toft (1999), Evolution of the depleted mantle: Hf isotope evidence from juvenile rocks through time, *Geochim. Cosmochim. Acta*, *63*, 533–556, doi:10.1016/S0016-7037(98)00274-9.

Vervoort, J. D., P. J. Patchett, U. Söderlund, and M. Baker (2004), The isotopic composition of Yb and the precise and accurate determination of Lu concentrations and Lu/Hf ratios by isotope dilution using MC-ICP-MS, *Geochem. Geophys. Geosyst.*, *5*, Q11002, doi:10.1029/2004GC000721.

Von Tish, D. B., R. W. Allmendinger, and J. W. Sharp (1985), History of Cenozoic extension in central Sevier Desert, west-central Utah, from COCORP seismic reflection data, *Am. Assoc. Pet. Geol. Bull.*, *69*, 1077–1087.

Wallis, S. R., J. P. Platt, and S. D. Knott (1993), Recognition of syn-convergence extension in accretionary wedges with examples from the Calabrian Arc and the eastern Alps, *Am. J. Sci.*, *293*, 463–494, doi:10.2475/ajs.293.5.463.

Wells, M. L. (1997), Alternating contraction and extension in the hinterlands of orogenic belts: An example from the Raft River Mountains, Utah, *Geol. Soc. Am. Bull.*, *109*, 107–126, doi:10.1130/0016-7606(1997)109<0107:ACAEIT>2.3.CO;2.

Wells, M. L. (2011), Eocene to Miocene history of the Middle Mountain shear zone system, *Geol. Soc. Am. Abstr. Programs*, *43*, 49.

Wells, M. L., and T. D. Hoisch (2008), The role of mantle delamination in widespread Late Cretaceous extension and magmatism in the Cordilleran orogen, Western US, *Geol. Soc. Am. Bull.*, *120*, 515–530, doi:10.1130/B26006.1.

Wells, M. L., J. S. Struthers, L. W. Snee, J. D. Walker, A. E. Blythe, and D. M. Miller (1997), Miocene extensional reactivation of an Eocene extensional shear zone, Grouse Creek Mountains, Utah, *Geol. Soc. Am. Abstr. Programs*, *29*, A-162.

Wells, M. L., T. D. Hoisch, M. P. Peters, D. M. Miller, E. W. Wolff, and L. W. Hanson (1998), The Mahogany Peaks Fault, a Late Cretaceous–Early Paleocene normal fault in the hinterland of the Sevier Orogen, *J. Geol.*, *106*, 623–634, doi:10.1086/516046.

Wells, M. L., L. W. Snee, and A. E. Blythe (2000), Dating of major normal fault systems using thermochronology: An example from the Raft River detachment, Basin and Range, western United States, *J. Geophys. Res.*, *105*, 16,303–16,327, doi:10.1029/2000JB900094.

Wells, M. L., J. C. Sheeley, T. L. Spell, E. D. Kelly, and T. D. Hoisch (2004), Eocene extension in northwestern Utah-southern Idaho: Early motion on the polyphase Middle Mountain shear zone, *Geol. Soc. Am. Abstr. Programs*, *36*, 73.

Wells, M. L., M. A. Beyene, T. L. Spell, J. L. Kula, D. M. Miller, and K. A. Zanetti (2005), The Pinto shear zone, a Laramide extensional shear zone in the Mojave Desert region of the southwestern Cordilleran orogen, western United States, *J. Struct. Geol.*, *27*, 1697–1720, doi:10.1016/j.jsg.2005.03.005.

Wells, M. L., T. L. Spell, T. D. Hoisch, T. Arriola, and K. A. Zanetti (2008), Laserprobe $^{40}Ar/^{39}Ar$ dating of strain fringes: Mid-Cretaceous orogen-parallel extension in the interior of the Sevier orogen, *Tectonics*, *27*, TC3012, doi:10.1029/2007TC002153.

Wernicke, B. (1992), Cenozoic extensional tectonics of the U.S. Cordillera, in *The Cordilleran Orogen: Conterminous U.S.*, *Geol. North Am.*, vol. G-3, edited by B. C. Burchfiel, P. W. Lipman, and M. L. Zoback, pp. 553–581, Geol. Soc. of Am, Boulder, Colo.

Willett, S. D. (1992), Dynamic and kinematic growth and change of a Coulomb wedge, in *Thrust Tectonics*, edited by K. R. McClay, pp. 19–31, Chapman and Hall, London, doi:10.1007/978-94-011-3066-0_2.

Willett, S. D. (1999), Rheological dependence of extension in wedge models of convergent orogens, *Tectonophysics*, *305*, 419–435, doi:10.1016/S0040-1951(99)00034-7.

Wright, J. E., and J. L. Wooden (1991), New Sr, Nd, and Pb isotopic data from plutons in the northern Great Basin: Implications for crustal structure and granite petrogenesis in the hinterland of the Sevier thrust belt, *Geology*, *19*, 457–460, doi:10.1130/0091-7613(1991)019<0457:NSNAPI>2.3.CO;2.

Yonkee, W. A. (1992), Basement-cover relations, Sevier orogenic belt, northern Utah, *Geol. Soc. Am. Bull.*, *104*, 280–302, doi:10.1130/0016-7606(1992)104<0280:BCRSOB>2.3.CO;2.

Yonkee, W. A., P. G. DeCelles, and J. Coogan (1997), Kinematics and synorogenic sedimentation of the eastern frontal part of the Sevier orogenic wedge, northern Utah:, *Brigham Young Univ. Geol. Stud.*, *42*, 355–380.

Zhu, X. K., R. K. O'Nions, N. S. Belshaw, and A. J. Gibb (1997), Significance of in situ SIMS chronometry of zoned monazite from the Lewisian granulites, northwest Scotland, *Chem. Geol.*, *135*, 35–53, doi:10.1016/S0009-2541(96)00103-9.

A. M. Cruz-Uribe, Department of Geosciences, Pennsylvania State University, 542 Deike Bldg., University Park, PA 16802, USA.

T. D. Hoisch, Department of Geology, Northern Arizona University, PO Box 4099, Flagstaff, AZ 86011, USA.

J. D. Vervoort, School of Earth and Environmental Sciences, Washington State University, Pullman, WA 99164, USA.

M. L. Wells, Department of Geosciences, University of Nevada, Las Vegas, 4505 Maryland Pkwy., Las Vegas, NV 89154, USA. (michael.wells@unlv.edu)